CONTROLS OF BASEMENT FABRIC ON RIFT COUPLING AND DEVELOPMENT OF NORMAL FAULT GEOMETRIES: INSIGHTS FROM THE RUKWA – NORTH MALAWI RIFT

Erin Heilman[1]

Folarin Kolawole[2]

Estella A. Atekwana[3]*

Micah Mayle[1]

Mohamed G. Abdelsalam[1]

[1]*Boone Pickens School of Geology*
Oklahoma State University
Stillwater, Oklahoma, USA

[2]*ConocoPhillips School of Geology & Geophysics*
University of Oklahoma
Norman, Oklahoma, USA

[3]*Department of Geological Sciences*
College of Earth, Ocean, and Environment
University of Delaware
Newark, Delaware, USA

**Corresponding author email: atekwana@udel.edu*

August 2018

Highlights

- To the SW, newfound strike-slip fault links the Rukwa and North Malawi Rift (RNMRS)
- To the NE, RNMRS border faults, intervening faults and volcanic centers are colinear
- RNMRS border faults and transfer structures align with pre-existing basement fabrics
- Basement fabrics guide the development of normal fault geometries and rift bifurcation
- Basement fabrics facilitate the coupling of the RMRS border faults and transfer structures

ABSTRACT

The Rukwa Rift and North Malawi Rift Segments (RNMRS) both define a major rift-oblique segment of the East African Rift System (EARS), and although the two young rifts show colinear approaching geometries, they are often regarded as discrete rifts due to the presence of the intervening Mbozi Block uplift located in-between. This problem has been complicated by the dominance of the Rungwe volcanic features along the northeastern boundary of the Mbozi Block and lack of distinct normal faults along the southwestern boundary of the block. Here, we investigate the coupling of discrete rift segments during the onset of continental rifting, modulated by the control of pre-existing basement fabrics on the development of the border fault geometries and linkage across the intra-rift transfer zone. We utilized the Shuttle Radar Topography Mission Digital Elevation Models (SRTM-DEM) to investigate the morphological architecture of the rift domains; and aeromagnetic data and SRTM-DEM to assess the relationships between the rift structures and the pre-existing basement fabric (in plan-view). Our results show that the present-day morphology of the RNMRS is characterized by along-rift alternation of rift shoulder polarity, characteristic of coupled rift segments. Careful interpretation

of filtered aeromagnetic maps along the northeastern and southwestern boundaries of the RNMRS reveal striking alignment of the rift-bounding faults with colinear NW-SE-trending pre-existing basement fabrics. We find that rift coupling along the northeastern boundary of the Mbozi Block transfer zone is accommodated by magmatism utilizing pre-existing fault systems, whereas, coupling along the southwestern boundary is accommodated by a new-found dextral strike-slip fault. Additionally, we show how the configuration of the pre-existing basement fabrics may influence the development of rectilinear or curvilinear normal fault geometries (plan-view) along the rifts, and the formation of basin-scale rift bifurcation around basement inter-rift transfer zones. In summary, we suggest that the structural continuation of the boundary faults along the RNMRS, and their alignment with colinear basement fabrics demonstrate the influence of structural inheritance on the coupling and amalgamation of approaching rift segments.

1. INTRODUCTION

Pre-existing basement fabrics are often major facilitators of continental rifting environments. Mechanically, they represent areas of structural weakness that can become reactivated and allow rifts to propagate preferentially along them (e.g., Daly et al., 1989). Several studies have documented the relationships between rift faults and the pre-existing basement fabrics (e.g., Wheeler and Karson, 1989; Kinabo et al., 2007, 2008; Taylor et al., 2011; Phillips et al., 2016; Kolawole et al., 2018; Siuda et al., 2018). Further, recent studies have assessed the 3-dimensional relationship between pre-existing basement thrusts and intra-rift normal faults, revealing the control of the pre-existing basement structures on the nucleation and strain distribution along the normal faults (e.g., Collanega et al., 2018). In the Cenozoic East African Rift System (EARS), which is divided into an Eastern, a Western and a Southwestern Branch (Fig. 1A), several zones of well-developed basement fabric influence rifting. One of the best recently-documented examples highlighting the influence of the Precambrian basement shear zones on rifting in eastern Africa is the role of the Mwembeshi Shear Zone on the development of the Luangwa Rift (Fig. 1A; Sarafian et al., 2018). It was demonstrated that the Mwembeshi Shear Zone acted as lithospheric conduit for fluids to migrate up the lithosphere, thus facilitating the weakening and subsequent initiation of the Luangwa rift in the Permo-Triassic.

However, the relationship between rift segments along the western branch of the EARS and the Precambrian shear zones is rather complex and warrants detailed and careful examination. For example, the Precambrian NW-trending Aswa shear zone resulted in the termination (rather than facilitation) of the northeastward propagation of the Albertine-Rhino graben which represents the northern-most segment of the Western Branch (Katumwehe et al., 2015) (Fig. 1A). On a basin scale, previous studies have also shown that pre-existing basement

142 shear zones can influence the localization of fault development (e.g., Phillips et al., 2016;
143 Kolawole et al., 2018), and in fact control fault segmentation and across-basin strain transfer at
144 later stages of rift development (e.g., Muirhead and Kattenhorn, 2018).

145 The border faults along large continental rift systems, e.g., the EARS, are typically ~100
146 km long (e.g., Foster et al., 1997; Lao-Davila et al., 2015), and the development of such large
147 normal faults with complex segment linkage styles are yet to be fully understood (e.g., Fossen
148 and Rotevatn, 2016; Gawthorpe et al., 2003; Rotevatn et al., 2018). However, since the
149 interactions between the large normal faults within juvenile extensional tectonic settings lead to
150 the systematic coupling of rift segments across transfer zones (e.g., Corti, 2012), border fault
151 segmentation, geometries and continuity between rift segments can provide insight into the
152 larger process of coupling between the segments of a rift system.

153 In this study, we focus on the Rukwa-North Malawi segment of the EARS, which is a
154 major rift-oblique segment of the rift system and serves as the central segment of the system. For
155 simplicity, we here-in refer to the Rukwa - Northern Malawi Rift segment of the East African
156 Rift as the "RNMRS". This segment is composed of the Rukwa Rift basin, the North Malawi
157 Rift basin and the Mbozi Block which represents the accommodation zone between the two rifts
158 (Fig. 1B). We address the longstanding question of the role of long-lived pre-existing basement
159 structures in the development of the trends and geometries of rift-bounding faults, leading to
160 subsequent coupling of individual rift segments during the onset of continental rifting. We
161 demonstrate that there is continuous structural connectivity along the boundaries of the RNMRS,
162 modulated by reactivation of the Precambrian metamorphic fabrics, and show that the
163 characteristic plan-view geometries of the rift-bounding faults are modulated by the
164 configuration of the basement fabric.

2. GEOLOGIC SETTING

2.1. The Precambrian Domains

The Rukwa-North Malawi Rift Segment is located within the NW-trending Paleoproterozoic Ubendian orogenic belt which is sandwiched between the Archean Tanzanian craton in the northeast and the Bangweulu cratonic block to the southwest (Figs. 2A-B; Fritz et al., 2013). The Ubendian Belt is composed of different Precambrian terranes bounded by steep shear zones (Delvaux et al., 2012). These terranes contain granulite-facies metamorphic rocks (2100-2025 Ma), amphibolite-facies metamorphic rocks and granitoids (1960-1800 Ma) that have undergone dextral strike-slip shearing and granitic plutons (1090-1120 Ma), (Fritz et al., 2013). The Paleoproterozoic Usagaran orogenic belt that extends NE-SW perpendicular to the Ubendian orogenic belt in southern Tanzania, is composed of eclogites (~2000 Ma), volcano-sedimentary cover with some low-grade metamorphism (~1920 Ma), and granitoids and granitoid gneisses (1900-1730 Ma) (Fritz et al., 2013). The Usagaran and Ubendian orogenic belts resulted from collision with the Tanzania craton, where the Usagaran orogenic belt was thrust onto the craton and the Ubendian orogenic belt was accreted along the craton's margin because of strike-slip motion (Daly, 1988; Lenoir et al., 1994). The Ubendian Belt was reactivated several times, preserving geochronologic, and petrographic and geochemical evidences of successive terrane accretion (e.g., Lenoir et al., 1994; Boniface and Schenk, 2012; Boniface et al., 2012). Known terranes within the Ubendian Belt are separated by shear zones which include the Mughese Shear Zone and the Mtose Shear Zone (Fig. 2; Daly, 1988; Delvaux et al., 2012), where the Chisi Suture Zone represents the major suture zone between the Precambrian Tanzania Craton and Bangweulu Block (Boniface and Schenk, 2012). Recent studies have highlighted the role of these shear zones in fault development (e.g., Morley, 2010; Delvaux et al., 2012; Kolawole et al.,

188 2018) and the distribution of seismicity in southern Tanzania and northern Malawi (Dawson et
189 al. 2017; Kolawole et al., 2018).
190
191 *2.2. The Rukwa Rift, Northern Malawi Rift, and the Mbozi Block accommodation zone (RNMRS)*
192 The RNMRS evolved during the Permo-Triassic episode of rifting that affected southern and
193 eastern Africa, also known as Karoo rifting (Chorowicz, 2005). Outcrops of Karoo sediments
194 have been mapped along the southern end of the Rukwa Rift (Figure 2) and the northern section
195 of the North Malawi Rift Basin (Kilembe and Rosendahl, 1992). These sediments lie
196 unconformably over the Precambrian basement and consist mainly of sandstone, shale, and coal
197 and thicken towards the border faults providing evidence for reactivation of synthetic faulting in
198 the Permo-Triassic (Morley, 1992; Delvaux et al., 1992).
199 Cenozoic rifting began in the Upper Miocene, characterized by normal faulting and basin
200 subsidence with the diagenesis of Red Sandstones and Lake Bed Sediments (Delvaux and
201 Hanon, 1991). Additional subsidence occurred after the deposition of these packages, and in
202 different directions, evidenced by the drag orientations of sediment packages on the faults
203 (Kilembe and Rosendahl, 1992). The Cenozoic rifting featured the reactivation of older faults as
204 seen in seismic profiles of the Rukwa Rift in which the faults are mostly contiguous from Karoo
205 sediments to Red Sandstones to Lake Beds (Kervyn et al., 2006). The present-day tectonic
206 activity in the RNMRS consists of limited volcanic eruptions, minor seismicity in the Mbozi
207 Block region, and continued sedimentation in the Rukwa and North Malawi basins (Delvaux and
208 Hanon, 1991).
209 The present-day architecture of the RNMRS consists of the Rukwa Rift to the northwest
210 of the segment, with the Lupa Fault (generally considered the border fault) bounding it to the

211 northeast and the Ufipa Fault to the SW (Fig. 1B). Towards the southeastern end of the Rukwa
212 Rift. It bifurcates around the Mbozi Block forming the Songwe Trough (ST) to the northeast and
213 the Musangano Trough (MT) to the southwest. The Mbozi Block transitions into the North
214 Malawi Rift (also known as the North Basin) which represents the southeastern end of the
215 RNMRS and it consists of a half-graben, bounded to the northeast by the Livingstone Fault (Fig.
216 1B). The Mbozi Block is referred to as an accommodation zone because it is thought to
217 accommodate and transfer relative strain between the Rukwa and North Malawi Rift Basins
218 (Delvaux and Hanon, 1993)

219 The Mbozi is a mass of Precambrian basement that is composed of Meta-basites and
220 intermediate granulites and quartzites of the Mbozi Terrane (Daly, 1988) and is bounded to the
221 southwestern by the Mughese Shear Zone (Fig. 2B), and overlain on the northeast by the
222 volcanic deposits of the Rungwe Volcanic Province (RVP). The RVP is a ~1500 km^2 area of
223 volcanic rocks and structures that evolved ca. 9 Ma (e.g., Fontijn et al., 2012), and a strong
224 tectonic control on the localization of volcanic centers have been inferred (e.g., Fontijn et al.,
225 2010, 2012). To the northeast of the RVP, a poorly defined NE-trending rift basin occurs, known
226 as the "Usangu Basin", where Permo-Triassic to Recent sedimentary rocks overlie the
227 Precambrian basement (Mbede, 2002).

228 The crustal thickness beneath the Rukwa Rift is ~37.5 km (Kim et al., 2009), but varies
229 between ~33 km and ~39 km along the rift shoulder (Ufipa Plateau) (Hodgson et al., 2017), and
230 increases slightly to 41.1–42.1 km in the northwestern-most part of the rift where the rifting is
231 minimal. These suggest that overall, the crustal thinning beneath the rift has been minimal but
232 may be slightly more beneath the Songwe Trough (Njinju et al., 2018). Camelbeeck and Iranga
233 (1996) estimated ~42 km crustal thickness beneath the Songwe Trough. Whereas, an average

crustal thickness of 39 km has been estimated for the Rungwe Volcanic Province, ~37-39 km for the North Malawi Rift, and 38-42 km for the Proterozoic terrains surrounding the North Malawi Rift (Borrego et al., 2016; Njinju et al., 2018).

2.3. Kinematics of the RNMRS

The mode of opening of the Rukwa Rift – Northern Malawi Rift segment is controversial. Overall, two models have been proposed. One of the models advocates for orthogonal rifting due to the dominance of NW-trending pre-existing basement fabric in the region, which resulted in the rotation of the E-W directed regional extension into NE-SW, thus producing NW-striking normal faults (e.g., Delvaux et al., 1992; Morley, 2010; Delvaux et al., 2012). The other model argues for oblique extension primarily due to the obliqueness of the rift segment to the E-W directed extension, thus resulting in the development of NW-trending dextral strike-slip faults (e.g., Chorowicz, 1989; Daly et al., 1989; Wheeler and Karson, 1994; Kervyn et al., 2006; Mortimer et al., 2007). Both models are based on observations from only the Rukwa Rift and North Malawi Rifts, and did not consider the kinematics of brittle structures along the Mbozi Block accommodation zone.

3.0 MATERIAL AND METHODS

In this study, we carried out detailed mapping of exposed and buried fault segments within the RNMRS. We utilized Shuttle Radar Topography Mission (SRTM) Digital Elevation Model (DEM) to locate surface expressions of faults; and filtered aeromagnetic data to map the plan-view trace of basement faults and metamorphic fabrics.

3.1. SRTM DEM Data

We extracted topographical profiles along the length of the rift from the SRTM DEM data to investigate surface morphology of the rift segments which could provide insight into the evolving nature of the rift architecture along the RNMRS.

3.2. Aeromagnetic Data

We combined three separate aeromagnetic surveys consisting of data acquired over northeastern Zambia, southern Tanzania and Northern Malawi. The Tanzania survey was collected between 1977-1980 with flight height of 200 m and a flight line spacing of 1 km. The Zambia survey was collected between 1973-1976 with a flight height of 150 m and a flight line spacing of 800-1000 m. The Malawi survey was carried out in 2013 with a flight height of 80 m, a flight line spacing of 250 m. Before merging the three surveys, we first corrected for the skewness of the data by reducing each of them to the magnetic pole (RTP). The RTP correction normalizes the magnetic field to the magnetic field at the pole so the anomalies retain their correct strike and shape, allowing the magnetic data to be interpreted as geologic structures (Baranov, 1957; Silva, 1986). Afterwards, we applied upward-continuation (Henderson and Zeitz, 1949) of 120 m to the RTP-corrected Malawi data, 50 m to the Zambia data in order to mathematically normalize the three datasets to a 200 m observational height. We then merged the three surveys into a single aeromagnetic grid file. Further, we applied the vertical derivative (VDR) filter to the merged data in order to enhance magnetic gradients associated with possible basement faults and basement metamorphic fabrics (Salem et al., 2008).

The vertical derivative edge filter has been very effective in the mapping of plan-view trace of buried active faults from aeromagnetic data in different parts of the EARS (Kinabo et al.,

2007, 2008; Kolawole et al., 2017, 2018). Excluding the Rungwe Volcanic Province (RVP; Figure 3) where volcanic materials overlie the crystalline basement, there is no information on the presence of basaltic rocks along the fault segments interpreted in this study. Therefore, we assume induced magnetization as the primary source of magnetization, except in the Rungwe Volcanic Province (RVP) where volcanic deposits are present. However, we do not have information on remanent magnetization in the RVP at this time. Due to the higher spatial resolution of the Malawi aeromagnetic data (62 m grid cell size) compared to those covering Zambia (225 m grid cell size) and Tanzania (250 m grid cell size), the magnetic anomalies are most significantly better resolved in the Malawi part of the filtered aeromagnetic maps.

4.0 RESULTS

4.1. Variation in rift morphology from topographic profiles

We examined fifteen rift-orthogonal topographic profiles (spaced at 40 km) along the RNMRS (Fig. 1B) to understand the overall along-strike variation in rift morphology. The investigation of rift dynamics by careful analyses of the topographic structures has provided important information on the subsurface architecture of rift systems (e.g., Pik et al., 2008; Wichura et al., 2011; Lao-Davila et al., 2015). Our morphological assessments focus on the variation in the scarp-heights (relief above the surface) of exposed normal faults along the RMNRS. This provides the minimum estimate of the relative vertical displacements of the faults at the point of assessment, hence the term ‘exposed minimum vertical displacement’ (EMVD) (Lao-Davila et al., 2015).

Profile 1 (Fig. 3), obtained at the northern tip of the Rukwa Rift shows no pronounced fault scarps, and the slight topographic high between Lake Tanganyika and Ufipa Fault

represents the northernmost tip of the Ufipa Plateau. In Profile 2, the surface morphology of the rift shows sharp topographic gradients bounding the Rukwa Rift Valley. These topographic gradients correspond to the scarps of the Ufipa Fault (600 m) and the Lupa Fault (750 m). In this northern part of the Rukwa Rift, the Ufipa and Lupa Faults have comparable scarp heights, thus illustrating a typical graben structure. In Profile 3, the rift structure changes into a half-graben surface morphology with the Ufipa Fault having a significantly higher escarpment than the Lupa Fault (~900 m difference). Profiles 4 to 7 show the same half-graben morphology for the Rukwa Rift as in Profile 3; however, we observe that the Ufipa Fault scarp is much higher than the topography of the Ufipa Plateau to its west along Profile 4.

Along Profiles 6 and 7, we observe that the Ufipa Fault scarp is lower than in the northern profiles (Profiles 1-5) and that the Lupa Fault scarp is also higher than in the northern profiles. In Profile 7, the Rukwa Rift splits into two basins separated by the Mbozi Block such that the west basin (Musangano Trough) is bound by the Ufipa Fault to the southwest, and the east basin (Songwe Trough) is bound by the Lupa Fault to the northeast. Profiles 7 to 9 shows a continuous southeastward decrease in the scarp heights of the Ufipa and Lupa Faults; and although the Ufipa Fault scarp is still visible south of the Mbozi Block along Profile 9, the Lupa Fault scarp is significantly diminished. Profile 9 shows a gentle topographic transition from the Musangano Trough to the Mbozi Block, but to the northeast of the Mbozi Block, the topography spikes abruptly, representing the northern limits of the Rungwe Volcanic Province (RVP). In Profile 10, the Ufipa Fault bounds what appears to be the southernmost extent of the Musangano Trough, while the uplifted Mbozi – RVP domain dominates the terrain and drops off into the Usangu Trough to the northeast. Profile 11 transects the northernmost tip of the North Malawi Rift, where the RVP (bounded to the northeast by the Livingstone Fault scarp) represents the

most dominant structure in the terrain and the entire topography of the Mbozi Block and areas to its southwest are relatively lower.

Profiles 12 and 13 illustrate half-graben morphologies for the North Malawi Rift (North Basin) with the Livingstone Fault (northeast bounding fault) dominating the topography. Profile 14 transects the transfer zone between the North and Usisya Basins of the Malawi Rift showing both the Livingstone border fault to the northeast and the Nyika Plateau to the southwest. Profile 15 which transects the Usisya Basin describes a half-graben surface morphology but in which the rift bounding fault is located on the southwest.

4.2. Aeromagnetic lineaments and basement fabric

The RTP merged (Fig. 4A) and edge-enhanced (Fig. 4B) aeromagnetic maps over the RNMRS provide a continuous plan-view image of the basement structures along the rift segment. Although the Malawi part of the merged data has the highest resolution, the moderate resolution of the Tanzania and Zambia parts of the data allows for considerable delineation of the trends of magnetic anomalies. Overall, the areas of basement exposures exhibit high amplitude, high frequency and short wavelength magnetic anomalies that delineate lineaments of interpretable trends (e.g., Kolawole et al., 2018). The high frequency lineaments can be easily observed on the rift shoulders of the Rukwa and North Malawi Rifts (Fig. 4B), and are commonly truncated at the rift margins by the rift-bounding faults (black arrows in Fig. 4B).

Within the rift valleys where sedimentary rocks overlie the deeply-buried basement rocks, the detailed magnetic fabric of the basement becomes suppressed such that gradients in the magnetic data could correspond to fault offset within the magnetic source (e.g., Grauch and Hudson, 2007, 2011; Kolawole et al., 2018) or remnants of the suppressed magnetic foliation of

the source (Kolawole et al., 2018). In the study area, the magnetic anomalies within the rift basins are dominated by relatively lower amplitude, longer wavelength and lower frequency anomalies.

4.3. SRTM DEM Fault trends and Aeromagnetic lineaments

We compare the along-axis geometry of the rift-bounding faults (from SRTM DEM) with the metamorphic fabric (in plan view) of the host basement rocks along the rift shoulders (from filtered aeromagnetic data) (Figs. 5-11). Figures 5-9 focus on the southwestern boundary of the RNMRS, consisting of the Ufipa Fault of the Rukwa Rift, the southwestern boundary of the Mbozi Block and the southwestern boundary faults of the North Malawi Rift. Whereas, Figures 10 and 11 focus on the northeastern boundary of the RNMRS, consisting of the Lupa Fault of Rukwa Rift, the northeastern boundary of the Mbozi Block (i.e. the Rungwe Volcanic Province) and the Livingstone Fault of the North Malawi Rift. We constrain our identification of the Precambrian terranes and strike of their fabrics with previous field studies of the Precambrian basement along the RNMRS (e.g., Daly, 1988; Wheeler and Karson, 1989; Lenoir et al., 1994; Theunissen et al., 1996; Boven et al., 1999; Fernandez-Alonso et al., 2001; Ring et al., 2002; Boniface and Schenk, 2012; Delvaux et al., 2012, Lawley et al., 2013; Kolawole et al., 2018). Overall, within the study area, we observe that the basement fabrics exhibit two styles, (1) discrete fabrics which include isolated magnetic lineaments of strong amplitude; and (2) distributed fabrics which encompass fabric sets of multiple medium-to-low amplitude magnetic lineaments as distributed fabrics.

4.3.1. Southwestern boundary of the RNMRS

In the northernmost part of SW Rukwa Rift (Chisi area) (Figs. 5A-C), we observe curvilinear fault geometries that follow Precambrian fabric (e.g., Ufipa, Chisi, Kalambo and Kanda Faults). In the Chisi area, the Rukwa Rift border fault consists of the Northern Ufipa Fault segment and the Chisi Fault segment. The tip of the Northern Ufipa Fault segment terminates against the WNW-ESE Chisi Fault at a high angle (Fig. 5A). The Chisi Fault aligns with a strong WNW-ESE magnetic-high lineament (discrete fabric) (Fig. 5B-C) consistent with the Chisi Suture Zone, which extends eastward into the rift basin (Theunissen et al., 1996; Boven et al., 1999; Boniface and Schenk, 2012; Fig. 2B). Also, the truncated Ufipa Fault segment aligns with the Ufipa Terrane basement fabrics (distributed fabrics). The North Ufipa Fault and Chisi Fault link at a very high angle to form a salient that point basinward (the Chisi Salient).

In the central part of the Ufipa Fault (Figs. 6A-C), the fault segments also exhibit curvilinear geometries and the hard linkage of major fault segments occur at high angles (e.g., Kwera relay ramp). The Kwera relay ramp is the largest relay zone along the Ufipa Fault. To the north of the Kwera relay ramp, the fault trends parallel to a magnetic lineament (discrete fabric) that is located to its east, whereas, to the west of this fault segment, the basement is characterized by two cross-cutting sets (NNW-SSE and NW-SE) of distributed fabrics. The NNW-SSE set represent the fabrics of the Ufipa Terrane, but the origin NW-SE is unknown at this time. The Ufipa Fault segments appear to follow the NNW-SSE basement fabrics but side-steps by means of short fault segments that align with the NW-SE fabric set. To the south of the relay ramp, the Ufipa Fault strikes parallel to the Mughese Shear Zone fabric which is colinear with the NNW-SSE set.

Towards the southern part of the Ufipa Fault, in Figures 7A-C, we observe that the Ufipa Fault segments exhibit rectilinear geometries such that it is difficult to delineate fault

bends that could correspond to breached relay ramps. In addition, we observe a stronger alignment of the Ufipa Fault segments with the Mughese Shear Zone fabric within the area. To the east of the Ufipa Fault, a fault that strikes parallel to the Ufipa Fault separates the Musangano Trough from the Mbozi Block. The Mbozi basement is characterized by metamorphic fabrics that strike WNW-ESE to NW-SE, oblique to the fault but in which subtle bends in the fault trend align with the basement fabric.

In the southern part of the Ufipa Fault (Figs. 8A-C), the fault is characterized by two segments. One of the segments represents a rectilinear southward continuation of the Ufipa Fault and is bounded to the east by a linear ridge that separates it from the Musangano Trough (see "Mughese Fault" segment at Tunduma in Figs. 8A-C). The other segment splays away from the former and delineates a curvilinear geometry that looks like those in the northern and central segments of the Ufipa Fault; this curvilinear segment bounds the southernmost part of the Musangano Trough (see "Ufipa Fault" in Figs. 8A-C). Around Kaseye town (see Fig. 8A), the basement is partially buried and more deeply buried around Chitipa to the south. The continuation of the Ufipa Fault is only evident in the aeromagnetic data as a strong magnetic-low lineament that is bounded by bands of magnetic-high lineaments (see magnetic fabrics around Kaseye town in Fig. 8B). Within the Kaseye area, the NW-striking Mughese Shear Zone fabrics are truncated by a discrete N-S trending magnetic-high lineament (see area within purple rectangle in Fig 8C). The magnetic-low lineament that projects as a southward continuation of the Ufipa Fault persists along the Mughese Shear Zone fabric into the Karonga area of the North Basin of Malawi Rift where the Mughese Shear Zone is abruptly truncated by the Karonga Fault (KF in Fig. 8C). The Mbozi Terrane fabric strike NW-SE, at low angles to the trend of the Mughese Shear Zone.

Detailed analyses of the onshore faults along the hinge zone of the Northern Malawi Rift (Karonga area) are well documented in Kolawole et al. (2018). Major onshore hinge zone faults include the Karonga Fault (KF), St. Mary Fault (SMF), Kaporo Fault (KPF), Lupaso Fault (LF), Katesula Fault (KTF) and the Mbiri Fault (Figs. 9A-C). Although the Karonga Fault cuts the basement fabric, several basement-rooted buried fault segments along the rift margin align with the fabric of the Mughese Shear Zone (Kolawole et al., 2018). It is interesting to note that the Mbiri Fault, the longest fault (and potentially has the largest throw?) along the rift margin is sub-parallel to the strike of the continuation of the Ufipa Fault into the area ("Mughese Fault" in Fig. 9C). Although segments of the Mbiri Fault appear to align with the Mughese Shear Zone fabic, it is not clear if the fault reactivated the southwestern boundary of the shear zone or if the fault partially aligns with the fabric of the shear zone. However, we observe that for the most part, the side-steps along the Mbiri Fault align with the basement fabric.

4.3.2. Northeastern boundary of the RNMRS

In the northern part of the Lupa Fault, the fault trend defines long, rectilinear segments (Fig. 10A) and aligns with the Katuma Terrane, similar to those observed in the southern part of the Ufipa Fault where faults align with the trend of the Ufipa Terrane (Fig. 7). Although, the E-W trending fabric of the Usagaran Orogenic Belt dominates the aeromagnetic data along the northeastern Rukwa Rift shoulder (Fig. 10B), we also observe that closer to the Lupa Fault scarp, there are some lineaments that align with the fault. To the southwest of the Lupa Fault (within the rift valley), a strong magnetic-high lineament which correspond to the Chisi Suture Zone (see onshore continuation and outcrop of the shear zone in Fig. 5), strike sub-parallel to the trend of the Lupa Fault, but deviates more significantly southwards (Figs. 4B and 10).

441 The southern part of the Lupa Fault (between the Katuma Terrane and the Rungwe
442 Volcanic Province) is characterized by curvilinear fault segments (Fig. 10 and 11). The Lupa
443 Terrane fabrics are oriented WNW-ESE, oblique to the Lupa Fault trend (Figs. 11A-C).
444 However, subtle steps along the curvilinear fault segments align with the Lupa Terrane fabrics.
445 In the Rungwe Volcanic Province (RVP), the magnetic lineaments strike NW-SE (Fig.
446 11B), similar to those of the Mbozi Terrane (8B and C), and are truncated to the west by a strong
447 NNW-striking magnetic high lineament (white arrows in Fig. 11B). Furthermore, we observe
448 that the volcanic centers align with NNW-striking magnetic gradient superimposed on the NW-
449 striking fabrics (black arrows in Fig. 11B). South of the Rungwe Volcanic Province, segments of
450 the Livingstone Fault system describe rectilinear geometries and align with strong magnetic-high
451 lineaments (shear zone?) in the Upangwa Terrane.
452
453 **5.0 DISCUSSION**
454 *5.1. Rift architecture*
455 The present morphology of the RNMRS reflects the result of multiple episodes of rifting that
456 have affected this part of eastern Africa i.e. a Permo-Triassic rifting episode (Karoo), a
457 Cretaceous episode and the ongoing Cenozoic rifting episode (e.g., Castaing, 1991; Morley et al.,
458 1992). The Rukwa Rift has been described as both a graben (e.g., Zhao et al., 1997) and half-
459 graben (e.g., Kilembe and Rosendahl, 1992) bounded by the oppositely-dipping Ufipa and Lupa
460 normal faults. The Lupa Fault is commonly regarded as the major border fault of the Rukwa Rift
461 due to its larger throw of ~7 km (Peirce and Lipkov, 1988) relative to the Ufipa Fault (Fig. 12);
462 however, it has also been shown that the Cretaceous and Cenozoic sediments in the rift thicken
463 towards both faults (Fig. 12; Morley et al., 1992; Zhao et al., 1997). In this study, our

topographical assessments (Fig. 3, profiles 1-7) show that the scarp height of the Ufipa Fault consistently exceeds that of the Lupa Fault through-out the rift segment, thus suggesting significant footwall uplift along the Ufipa Fault.

The significantly lower scarp-height of the Lupa Fault suggests either that it has not been very active in Cenozoic times or that it has been heavily eroded since the cessation of Mesozoic rifting. However, based on these observations, we interpret that in the earlier rifting episodes (especially in the Permo-Triassic Karoo episode), the Lupa Fault played the role of the major border fault such that the basin defines a typical half-graben geometry; but in the present Cenozoic phase of rifting, the Ufipa Fault appear to have been preferentially accommodating more strain. Therefore, we suggest that the Rukwa Rift is possibly transitioning into an asymmetric-graben geometry. An asymmetric-graben is a graben with EMVD greater on one border fault compared to the other one, such that the basin polarity has shifted to the fault with the greater 'exposed minimum vertical displacement' (EMVD) (Lao-Davila et al., 2015). The implications of the present Rukwa Rift morphology on the Lupa Fault may reflect temporal and spatial migration of strain accommodation from a previously dominant border fault into another one that has been previously less-dominant. This could possibly be explained by the Scholz and Contreras (1998) suggestion that when a rift-bounding fault attains some limiting offset, motion on the fault will cease, and strain will be transferred to a new fault.

5.2. The Southwestern Boundary of the RNMRS and relationships with Precambrian Basement Fabric

In the Chisi area, the Northern Ufipa Fault segment terminates against the Chisi Suture Zone along which the Chisi Fault segment developed. The termination of the Ufipa Fault at its

intersection with this shear zone exemplifies one of the roles of pre-existing basement structures as temporal and/or spatial mechanical 'barriers' that arrest and delimit the continuous lateral propagation of a fault. Several studies on fracture propagation have demonstrated that fractures are principally bifurcated, blunted, and/or arrested when they intersect discontinuities, stress barriers and/or rock layers of significantly-contrasting mechanical properties along their path of propagation (e.g., Helgeson and Aydin, 1991; Gudmundsson and Brenner, 2001; Zhang et al., 2007; Zhang and Jeffrey, 2008). Other examples of normal fault termination at long-lived basement shear zones include the case of the Albertine-Rhino Graben terminating at the Aswa Shear Zone (Katumwehe et al., 2015) and the Okavango Rift border faults against the Sekaka Shear Zone (Modisi et al., 2000). We suggest that both the reactivation of the Chisi Suture Zone into the Chisi Fault and termination of fault segments at the shear zone demonstrate the strong influence of the Chisi Suture Zone on the development of this part of the Rukwa Rift.

Although the northern segments of the Ufipa Fault align with the basement fabrics (Fig. 5B-C) and the southern segments show even stronger alignment with the NNW-SSE fabrics of the Ufipa Terrane and/or Mughese Shear Zone (Fig. 7), we find that the central segments of the fault show only partial alignment with this basement fabric (Fig. 6A-C). These observations imply that, although the Ufipa Fault is thought to have largely propagated along the Mughese Shear Zone (Fig. 2; Delvaux et al., 2012), there is stronger control of the Mughese Shear Zone and Ufipa Terrane fabrics on the fault development along its northern and southern segments than in the central part. We suggest that the partial control of these NNW-SSE fabrics on the central Ufipa Fault segments is due to the occurrence of a NW-SE basement fabric set on the Mughese Shear Zone and Ufipa Terrane fabric (Fig. 6). This may also explain the localization of the largest relay zone along the Ufipa Fault at its central segment.

510 The Tunduma-Kaseye area of Malawi, through the Misuku Mountains (Fig. 8A)
511 constitute the southern boundary of the Mbozi Block. Although, the SRTM DEM shows that the
512 sub-aerial expression of the Ufipa Fault dies out roughly mid-way between Tunduma and
513 Kaseye, the filtered aeromagnetic data reveals that in the subsurface, the fault continues across
514 the Kaseye-Chitipa area as a distinct magnetic-low lineament that bounds the Mughese Shear
515 Zone to the south and runs southeastwards into the Karonga area (Fig. 8B). Upon closer
516 observation of the continuation of this strong magnetic-low lineament in the Kaseye-Chitipa
517 area, we find that it cuts-across and offsets a N-S striking magnetic-high lineament which
518 extends 80 km southwards into the Permo-Triassic Luangwa Rift in Zambia. We interpret this N-
519 S lineament as a mafic dike that is possibly related to one of the earlier (Triassic or Cretaceous)
520 episodes of rifting which are known to have been associated with extensive late-stage diking
521 events in the Luangwa Rift (e.g., Van de Velde and De Waele, 1998) and Shire Graben in
522 southern Malawi (Castaing, 1991). Sedimentary deposits in the Kaseye-Chitipa area resulted in
523 the burial and lack of sub-aerial exposure of this structure, thus making this study the first
524 revelation of its existence in Northwestern Malawi.

525 Our analyses of the geometry of the interpreted dike structure (Fig. 13A), here in referred
526 to as the Chitipa Dike, shows a distinct difference in the geometry of the structure to the north
527 where it is cut by the strong magnetic-low lineament (continuation of the Ufipa Fault) and to the
528 south (farther away from the fault intersection). South of Chitipa (Fig. 13B), we observe that the
529 north-trending dike describes a consistent left-stepping geometry which diminishes across the
530 Chitipa town location and continues with a more rectilinear geometry northwards into the
531 Mughese Shear Zone area. This side-stepping geometry is typical of vertical sheet intrusions and
532 are related to either magma intrusion into pre-existing stepped joint systems (e.g., Baer, 1991) or

near-surface stress rotations during magma intrusion (e.g., Fossen, 2010). In this study, the coincidence and strike of the dike-steps along the NW- to NNW- striking basement fabric may in fact suggest the possible influence of pre-existing basement fabric on the stepping geometries of dike intrusions during their emplacement in host metamorphic rocks (Fig. 13B).

Further north, where the dike is cut by the continuation of the Ufipa Fault, the filtered aeromagnetic data shows the dike exhibiting consistent right-lateral offsets across NW-SE magnetic gradients (Fig. 13C). This clear distinction in the structural style of the dike south of Chitipa and in the north across the continuation of the Ufipa Fault, suggest that the contrasting structural styles are associated with different geological processes. In a summary, we interpret that along the southern boundary of the Mbozi Block, the continuation of the Ufipa Fault, which itself aligns with the Mughese Shear Zone fabric (Fig. 8B-C), is a right-lateral strike-slip fault that displaced a N-S trending Mesozoic (?) dike intrusion (Fig. 13C). We further interpret that this strike-slip fault reactivated the Precambrian Mughese Shear Zone at some time post-Cretaceous (i.e. related to the present Cenozoic rifting phase), and therefore refer to it as the "Mughese Fault". This interpretation is further supported by the change in the morphological expression of the Ufipa Fault from a typical single-scarp style into a narrow linear valley-ridge style in the Tunduma area in the SRTM DEM (see "linear ridge" in Fig. 8A). The observed linear valley-ridge geomorphology is typical of active strike-slip fault zones (e.g., McCalpin et al., 2009). In addition, previous field studies in the area (Delvaux et al., 2012) observed strike-slip displacement on rock outcrops at Tunduma and Mbozi Quarry ("Q" in Fig. 8A). Using the Chitipa Dike as a strain marker, we observe that the offsets increase northwards across multiple splays of the Mughese Fault and estimate that the displacement is maximum at the major Mughese Fault trace (northernmost extent of the strike-slip fault zone). Since mafic intrusions

often produce magnetic anomalies larger than the actual size of the sources, it is practically impossible to estimate the true cumulative strike-slip displacement from the aeromagnetic data. Based on the lateral dike separation across the fault on our aeromagnetic data, we estimate a minimum of 500 m lateral displacement along the Mughese Fault (Fig. 13C). It is also possible that this estimated offset only represents the lateral component of an oblique-normal slip along the fault. In Figure 14, we present a conceptual model that summarizes our interpretation of the Chitipa Dike geometry and the interaction of the Mughese Fault with the dike.

However, in Tunduma area (Fig. 8A), the presence of discrete breaching of the linear ridge by stream channels suggest that the strike-slip displacement along the Mughese Fault is most-likely a short-lived event that occurred at some time in the past during the development of the RNMRS. The curvilinear fault scarp adjacent to the Mughese Fault at Tunduma shows single-scarp morphology (not linear-ridge morphology) typical of normal faults as seen on the other segments of the Ufipa Fault. Therefore, we interpret this curvilinear fault scarp as a possible old segment of the Ufipa Fault that was 'pirated' by the Mughese strike-slip fault; thus, suggesting a phase in which the Ufipa Fault accommodated strike-slip displacement.

Along the southwest margin of the North Malawi Rift (Karonga area), the Mughese Fault diffuses into a zone of wide-spread faulting where the southeast-ward bend of the Mughese Shear Zone controls the development of the normal faults and recent seismicity along the basin hinge margin (Fig. 9A-C) (Kolawole et al., 2018; Dawson et al., 2018). Further south of Karonga town, the NNW-striking Mbiri Fault is the dominant fault structure in terms of its length (and displacement?) along this part of the hinge zone of the North Malawi Rift. We do not observe any direct spatial connectivity between the Mughese Fault and the Mbiri Fault. However, based on the sub-parallel geometry of both faults and the structural dominance of the Mbiri Fault in the

area, we suggest that the Mbiri Fault could possibly represent a continuation of the Mughese Fault into the hinge zone of the Malawi Rift North Basin. It is also important to note that the Mbiri Fault is synthetic to the Livingstone border Fault. Following the observations and interpretations above, we suggest that there exists a well-developed continuous connectivity of rift-related structures along the southwestern boundary of the RNMRS, facilitated by the extent of the Mughese Shear Zone and the Ufipa Terrane. Interestingly, the linking of the oppositely-dipping Ufipa and Mbiri Faults by the Mughese strike-slip fault describes a structure that, overall, is similar to that of the Morley et al. (1990) convergent-approaching normal fault system.

5.3. The Northeastern Boundary of the RNMRS and relationships with Precambrian Basement Fabric

The northern segment of the Lupa Fault exhibits clear alignment with the trend of the Katuma Terrane (Fig. 10) and with a few interpretable magnetic lineaments (likely due to low resolution of the aeromagnetic data). We also note that the Lupa Fault is sub-parallel to the Chisi Suture Zone in this area. Farther south of the Lupa Fault (Kapalala-Kanga area; Figs. 10 A-C), the fault segments occur at a high angle to the Usagaran Belt and Lupa Terrane fabrics, thus indicating an apparent lack of control of pre-existing basement fabric on the propagation of the southern Lupa Fault, except in the coincidence of the fault steps with the trend of the basement fabrics.

The southern segment of the Lupa Fault transitions into the Rungwe Volcanic Province (RVP) where surficial cover of volcanic deposits obscures the southward continuation of the Lupa Fault (Fig. 11A). In addition, the presence of mafic volcanic deposits in the RVP (e.g., Fontijn et al., 2012) makes it difficult to make a reliable interpretation of the magnetic fabric of

602 the underlying Precambrian basement (Fig. 11B). However, we find that a distinct magnetic-high
603 lineament aligns with the Mbaka Fault surface trace (white arrows in Figs. 11A and 11B). Also,
604 the distribution of volcanic centers in the RVP show alignment with both the Mbaka Fault trace
605 and a subtle curvilinear gradient (black arrows in Fig. 11B). Further south, the curvilinear
606 gradient connects with the Livingstone Fault, the northeastern border fault of the North Malawi
607 Rift. This curvilinear gradient coincides with the location and extents of the so-called "Ngozi-
608 Rungwe Line" of Fontijn et al. (2010), described as a buried fault system that served as a conduit
609 for magmatic fluids to migrate to the surface volcanic vents. Therefore, although it is possible
610 that the magnetic anomalies in this area are affected by remanent magnetization from the
611 volcanic deposits, we interpret that this aeromagnetic gradient provides a possible subsurface
612 evidence of the fault system (Ngozi-Rungwe Line) that connects the Lupa Fault and the
613 Livingstone Fault across the RVP. The filtered aeromagnetic data and previous field studies
614 (e.g., Wheeler and Karson, 1989) shows that the Livingstone Fault segments align with and
615 reactivated the fabric of the Upangwa Terrane (Figs. 11B-C). The observations and
616 interpretations above suggest that there exists a well-developed continuous connectivity of rift-
617 related structures along the northeastern boundary of the RNMRS. However, the relationship
618 between the basement fabric and the buried faults beneath the volcanic deposits remains unclear.
619
620 *5.4. Implications for Rift Development*
621 *5.4.1. Rift Coupling*
622 In the Rukwa Rift, the substantial dominance of the Ufipa Fault rift shoulder over that of the
623 Lupa Fault may imply that the Ufipa Fault is the present-day active border fault of the Rukwa
624 Rift. This proposition may be supported by the hypocentral location of the 1994 Mw5.9 Rukwa

earthquake and its aftershoks with epicentral location in the northern part of the rift (Fig. 12; Zhao et al., 1997). The nodal planes of the earthquake focal mechanism solution are broadly consistent with the orientation of both the Lupa and Ufipa faults, and relative position of aftershocks to the main shock is well determined (Fig. 12; Zhao et al., 1997). Considering the uncertainty range of the earthquakes, the spatial distribution of the aftershocks relative to the main shock delineates a sub-horizontal fault zone that most fits the subsurface projection of the Ufipa Fault (Fig. 12). In addition, field investigations of the Kwera relay ramp (see Fig. 6 for location) revealed features that indicate recent activity along the Ufipa Fault (Delvaux et al., 2012). Camelbeeck and Iranga (1996) observed several lower crustal seismicity in the Rukwa Rift with most of the events clustering beneath the Songwe Trough and the Rungwe Volcanic Province (southern parts of the rift; Fig. 1B). The locations of the clusters suggest activity along the southern Lupa Fault and Mbeya Range Fault. However, since the scarp height (and throw?) of the Ufipa Fault decreases southwards (Fig. 3), and the throw on the Lupa Fault increases southwards (and rapidly along the Songwe Trough) (Morley et al., 1992), we infer that the present border fault role of the Ufipa Fault excludes the southermost parts of the Rukwa Rift.

It has also been observed that the early stage of continental rifting is typically characterized by the development of along-axis alternating polarity of rift segments, rift border faults, uplifted rift flanks (e.g., Bosworth, 1985; Rosendahl, 1987; Hayward and Ebinger, 1996; Lao-Davila et al., 2015). The zones of polarity changes (transfer/accommodation zones) serve to transfer extensional strain between the rift segments and link the border faults which often have variable structural styles and geometries (e.g., Morley et al., 1990; Wilson, 1999). Within young continental rift settings, interactions between these large border faults lead to the systematic coupling of border faults and rift segments across the transfer zones, and subsequent growth of

the rift system (e.g., Corti, 2012). Along the RNMRS, the alternating location of the of rift shoulder uplift (SW in Rukwa Rift and NE in North Malawi Rift), typical of coupled rift segments, suggest that the RNMRS can be considered a coupled rift segment. Further, our study here shows that there is in fact, continuous structural continuation along the northeastern and southwestern margins of the RNMRS, typical of a coupled rift segment. Although, studies in the EARS and illustrations of its rift segments had always assumed this to be true, we hereby provide evidence supporting it, for the first time. In the West Antarctic rift system, the localization of recent volcanism along transverse structures within an accommodation zone (the Discovery accommodation zone) suggests active structural interactions between the flanking rift segments (Wilson, 1999). Therefore, we further suggest that the focusing of Neogene volcanism (e.g., Fontijn et al., 2010, 2012) along the northeastern boundary faults of the Mbozi accommodation zone (Fig. 15A) may be indicative of the ongoing coupling of the Rukwa and North Malawi Rift's northeastern border faults.

5.4.2. Rift Kinematics

Several studies have suggested that the development of the RNMRS has been dominated by dextral strike-slip kinematics (e.g., Chorowicz, 1989; Daly et al., 1989; Wheeler and Karson, 1994; Kervyn et al., 2006; Mortimer et al., 2007). However, analyses of fault architecture, fault-kinematics, paleostress and present-day earthquake focal mechanism solution in the Rukwa Rift show that the present-architecture of the rift largely developed within a pure extensional setting with extension direction orthogonal to the trend of the RNMRS (Morley, 2010; Delvaux et al., 2012). Furthermore, Delvaux et al. (2012) observed dextral strike-slip faulting along the fault systems bounding the Rukwa Rift, but concluded that the strike-slip event was transitory and was

associated with an early Mesozoic transpressional event that resulted in the inversion of Karoo sediments. In this study, we observe the existence of a well-defined strike-slip fault bounding the SW margin of the Mbozi Block that reactivated the Precambrian Mughese Shear Zone. We also observe lack of present-day activity along the strike-slip fault, and that this fault displaced a buried mafic dike with at least 500 m of dextral offset.

In the absence of chronological data on the mapped dike, we posit that the dike is most-likely associated with the widespread late-Karoo dike swarms observed in the Luangwa Rift and Shire Graben (southern Malawi) (Castaing, 1991; Van de Velde and De Waele, 1998). We refer to this strike-slip fault as the "Mughese Fault", and the buried dike as the "Chitipa Dike". The Chitipa Dike, presented for the first time in this work, may constitute the most excellent record of strike-slip kinematics along the RNMRS. Although, our results agree with Delvaux et al. (2012) in that the strike-slip faulting along the RNMRS was short-lived, we suggest that future geochronological analyses of this intrusion may provide the most-reliable constraint on the timing of strike-slip faulting event. It is also interesting to note that if the Mughese strike-slip fault is post-Karoo, its development represents a late reactivation of the Mughese Shear Zone in the evolution of the RNMRS. However, late reactivation of rift-oblique basement shear zones is not uncommon in rift basins (e.g., Muirhead and Kattenhorn, 2018).

Following the considerations above, we present cartoons of the RNMRS, illustrating the continuous structural connectivity along the northeast and southwest boundaries guided by the basement fabrics (Fig. 15B), and possible subsurface geometries and interactions of the domain-bounding structures (Fig. 15B-E). The inferred dominance of the Ufipa Fault in the northern and central parts of the Rukwa Rift (Fig. 12) suggest possible truncation of the Lupa Fault at depth, such that the load of the basin hanging wall block is being carried by the Ufipa Fault (Fig. 15B).

694 However, seismic data is needed to confirm this interpretation. We illustrate a possible spatial
695 relationship between the RVP magma pathways and the Mbozi Block bounding faults in Figure
696 15C. In Figure 15D-E, we show a generalized basin geometry and flip in border fault polarity
697 from the Malawi Rift North Basin to the Usisya Basin. Overall, we posit that, along the
698 northeastern boundary of the Mbozi Block transfer zone strain is accommodated by magmatism
699 utilizing pre-existing fault systems, whereas, along the southwestern boundary, strain is
700 accommodated by dextral strike-slip faulting.
701
702 *5.5. Control of basement fabrics on normal fault geometries*
703 Overall, along the border faults of the Rukwa Rift, we find that strongly-curvilinear normal fault
704 geometries (in plan-view) occur in three distinct settings. One, in areas where the basement
705 fabrics describe high curvatures (>15°) (e.g., in the Chisi area, northern segment of the Lupa
706 Fault; Fig. 5). Second, in areas of superposition of discordant sets of basement fabrics, in which
707 the overall fault strike is parallel to one of the sets and relay ramp breach-faults follow the other
708 fabric set that is oblique to the overall fault strike (e.g., central segment of Ufipa Fault; Fig. 6).
709 Third, in areas where the faults propagate at high-angle to the strike of the basement fabrics (e.g.,
710 in the Kapalala-Kanga area, southern segment of the Lupa Fault; Fig. 10). In general, along the
711 RNMRS, we find that in areas where the basement fabrics show low curvatures (<10°), the fault
712 segments tend to describe long, rectilinear geometries with narrow or almost unidentifiable
713 breached-relay zones (e.g., Southern Ufipa Fault, Fig. 7; Mughese Fault, Fig. 8; Livingstone
714 Fault, Fig. 11). We suggest that the control of rectilinear (<10° curvature) basement fabrics on
715 the propagation of normal faults may result in the development of rectilinear fault segments with
716 greater likelihood of occurrence of narrow relay ramps and tip-to-tip fault linkage.

717 Curvilinear normal faults have been observed at various scales and at different
718 extensional tectonic settings (Fossen and Rotevatn, 2016). However, the first order curvilinear
719 normal faults are typically characterized by segment boundaries with salients (cusps) that plunge
720 basin-ward e.g., Salt-lake salient and Transverse Mountain salients of the Wasatch Fault in Utah
721 (Fig. 16A), and the Gullfaks salient in the North Sea (Fig. 16B) (Fossen and Rotevatn, 2016).
722 Also, the reported curvilinear faults show characteristic basin-ward concave geometries.
723 However, the South Oquirrh Mountains normal fault zone, although curvilinear (Wu and Bruhn,
724 1994), exhibits striking basin-ward convex geometry in which the cusps point into the footwall
725 of the fault (Fig. 16A). Wu and Bruhn (1994) suggested that convex curvilinear geometry of the
726 South Oquirrh Mountains normal fault zone developed by sequential propagation of the fault into
727 its foot-wall, guided by linkage across smaller en-echelon faults created by the lateral shear
728 components at the tips of the propagating fault. Here, in the Rukwa Rift, we observe both
729 convex- and concave-curvilinear normal fault geometries along the Ufipa and Lupa Faults. The
730 central Ufipa Fault (Fig. 6) and southern Lupa Fault (Kapalala-Mwambani area in Fig. 10A-C)
731 exhibit convex-curvilinear normal fault geometries, whereas the northern Ufipa Fault and the
732 Chisi Fault demonstrate concave-curvilinear fault geometries (linked at the Chisi salient) (Fig.
733 5). Also, we find striking similarities between the concave- and convex-curvilinear fault
734 geometries of the Rukwa Rift (Fig. 16C) with those in the southern Malawi Rift (Fig, 16D), the
735 Jurassic sedimentary sequence of the northern North Sea rift (Gullfaks area) (Fig. 16B), and the
736 Provo-Salt Lake City area (Fig. 16A). As show in Figure 16D, the segments of the Bilila-
737 Mtakataka Fault in southern Malawi Rift present excellent examples of convex-curvilinear
738 normal fault geometries (Jackson and Blekinsop, 1997). Recent studies on the relationships
739 between the basement fabrics and the Bilila-Mtakataka Fault segments (Johnson et al., 2018;

740 Hodge et al., 2018) show that some of the segments appear to align with the distributed basement
741 fabrics, while others cut across the basement fabrics.

742 Based on the observations above, we present conceptual models for the control of
743 various configurations of pre-existing basement fabrics on the development of curvilinear normal
744 fault plan-view geometries (Fig. 17). We show how discrete and distributed basement fabrics and
745 combinations of the two categories of fabrics can influence the plan-view geometry of normal
746 faults. However, there is need to better understand (1) the influence of the basement fabrics on
747 the geometries of curvilinear normal faults in 3-dimensions, (2) the influence of the extension
748 direction on the development of the observed curvilinear normal faults in areas where the
749 basement fabric present mechanical anisotropy.

750 Although, Fossen and Rotevatn (2016) provide evidence of subsidiary short-cut faulting
751 across a salient, suggesting an impending evolution of concave-curvilinear faults into rectilinear
752 faults, it is not yet clear if the model applies to convex-curvilinear normal faults since the two
753 styles of faults are geometrically different. However, the synthetic Bilila-Mtakataka and the
754 Chirobwe-Ncheu Faults (Fig. 16D) in southern Malawi Rift may provide some insight. Since the
755 Chirobwe-Ncheu Fault is older than the Bilila-Mtakataka Fault (Jackson and Blekinsop, 1997),
756 the rectilinear geometry of the Chirobwe-Ncheu Fault suggests that the apices of convex
757 curvilinear segments may likewise eventually get breached to form more-rectilinear fault
758 segments. Conversely, we observe the opposite of this model along the Lupa Fault, where the
759 more-rectilinear northern Lupa Fault has accommodated much less strain compared to its
760 curvilinear southern segment which has the most strain within the Rukwa Rift (Morley et al.,
761 1992). Therefore, we suggest that although the model of temporal progression from a curvilinear
762 to rectilinear fault geometry may apply to some large normal faults, it may not apply to others.

763

764 *5.6. Rift Bifurcation*

765 The basin scale splaying of the Rukwa Rift around the Mbozi Block into the Musangano
766 and Songwe Troughs (Fig. 1B) obviously represents a smaller-scale of rift bifurcation when
767 compared to the continental scale bifurcation of rift systems around microplates. Examples of
768 such continental-scale rift bifurcation include the branching of the East African Rift around the
769 Tanzania microplate into the western and eastern branches (Fig. 1A; e.g., Rosendahl, B.R., 1987;
770 Versfelt and Rosendahl, 1989), the Red Sea Rift around the Sinai microplate into the Gulf of
771 Suez Rift and Dead Sea Transform, and the South Atlantic Rift around the Sergipe microplate
772 into the Tucano-Recôncavo Rift and Sergipe-Alagoas Transform (e.g., Szatmari and Milani,
773 1999) (Figs. 18A-C). Based on scale distinction, we therefore refer to the continental rift-system
774 scale bifurcation as first (1^{st}) order rift bifurcation (Figs. 18A-C) and the rift-basin scale
775 bifurcation as second (2^{nd}) order rift bifurcation (Fig. 18D-F). Similar to the Rukwa Rift, 2^{nd}
776 order rift bifurcations are common along the East African Rift System. Examples include the
777 Southern Malawi Rift bifurcation around the Shire Horst, the Shire Graben bifurcation around
778 the Namalambo Horst, and the Albertine Graben bifurcation around the Rwenzori Block (Fig.
779 18B; e.g., Castaing, 1991; Koehn et al., 2008; Lao-Davila et al., 2015; Xue et al., 2017).

780 Regardless of scale, numerical models have showed that inherited structural
781 heterogeneity and lateral strength variations are key controls on rift bifurcation (e.g., Brune and
782 Autin, 2013; Brune et al., 2017). However, it appears that 1^{st} order bifurcations commonly occur
783 at the tip of pre-existing microcratonic blocks along the path of propagation of a continental rift
784 system (e.g., Fig. 18A). Also, 2^{nd} order bifurcations appear to occur at the transfer zones between
785 approaching rift segments, possibly due to a high tendency for the development of interfingering

fault blocks in the transfer zones between colinear approaching rift segments (Morley, 1995) and lateral rotation of the trapped blocks in the transfer zones between overlapping approaching rift segments (Koehn et al., 2008).

It is possible that the bifurcation of the Rukwa Rift around the Mbozi Block is related to the location of the block within the transfer zone of the colinear approaching Rukwa and North Malawi Rift segments. However, we suggest that the basement fabrics of the Ubendian Belt around the Mbozi Block transfer zone could be playing a complementary role in facilitating and guiding the intra-rift bifurcation of the Rukwa Rift around the block. Our filtered aeromagnetic map (Fig. 4B) shows that the block is dominated by a WNW-ESE and N-S fabrics. According to Daly (1988), the Meta-basites and intermediate granulites and quartzites of the Mbozi Block are characterized by lineations that trend NE-SW. These observations, however, suggest that the Mbozi Block fabrics strike at oblique to high-angles to the trend of the colinear fabrics of the basement terranes bounding the Mbozi Block (Katuma-Upangwa Terranes to the northeast, and those of the Ufipa Terrane to the southwest) and the main rift-bounding faults (the Lupa, Ufipa, Livingstone and Mughese Faults) (Fig. 15A). Therefore, we suggest that the colinear fabrics of the basement terranes surrounding the Mbozi Block which are already controlling the propagation and linking of the rift-bounding faults may be playing a significant role in guiding the bifurcation of the Rukwa Rift around the Mbozi Block (Figs. 4B, 7, 8 and 11).

6.0 CONCLUSIONS

Our topographic analyses of the morphology of the RNMRS and detailed study of the relationships between the pre-existing basement fabric and rift-related faults provide, for the first time, evidence supporting the coupling of the Rukwa and North Malawi Rift. Our topographic

analyses in the Rukwa Rift suggest that the Ufipa Fault is the present-day active border fault of the rift. We find that the Ufipa fault is the dominant topographic feature in the northern part of the RMNRS and diminishes as it encounters the Mbozi block where it becomes a strike slip fault (Mughese Fault), at which point the border fault polarity flips and the Livingstone Fault is the dominant fault in the southern part of the RNMRS.

Further, we demonstrate the continuity structures along the northeastern and southwestern margins of the RNMRS. We show that this structural connectivity across the Mbozi Block transfer zone between the rifts is guided by the pre-existing Precambrian terrane fabrics and associated shear zones. We show that the coupling of the RNMRS along the northeastern boundary of the Mbozi Block transfer zone is accommodated by magmatism along the linking faults, whereas, coupling along the southwestern boundary is accommodated by strike-slip faulting. Overall, we suggest that the continuation of the boundary faults along the RNMRS, and their alignment with colinear Precambrian basement fabric and shear zones indicate the influence of the pre-existing basement structures on the coupling and amalgamation of approaching colinear rift segments. On the basin-scale bifurcation of the Rukwa Rift, we infer that the discordance of the basement fabrics within the Mbozi Block transfer zone to those of the basement terranes bounding it may have facilitated the development of intra-rift bifurcation of the rift around the transfer zone.

Furthermore, we show the influence of pre-existing basement fabrics on the development of the RNMRS as evidenced in the geometry, termination and kinematics of the rift-bounding fault segments. Our observations suggest that curvilinear normal fault geometries developed in areas where the basement fabrics are either curvilinear, composed of superposed sets of differently-orientated fabrics, or not favorably oriented to the extensional stress field. Whereas,

long, rectilinear fault geometries with narrow or almost unidentifiable breached-relay zones developed in areas where the pre-existing basement fabrics are roughly rectilinear, suggesting the greater likelihood of occurrence of tip-to-tip linkage of fault segments.

Finally, we present the existence of a buried Pre-Cenozoic strike-slip-faulted mafic dike, which we suggest is potentially the most excellent record of strike-slip kinematics along the RNMRS. We further suggest that future geochronological analyses of this intrusion may provide the most-reliable constraint on the timing of the controversial strike-slip faulting event along the RNMRS.

Acknowledgements

This work was partially supported by the National Science Foundation (NSF) grant EAR10-09988 (awarded to E.A. Atekwana). Also, we acknowledge the Oklahoma State University (OSU) for the Niblack Scholarship awarded to Erin Heilman. We thank the Geological Survey Department of Malawi for allowing us to purchase the 2013 aeromagnetic data used in this study. We also thank the Zambia Geological Survey for allowing us to purchase the aeromagnetic data used in this study. We thank South African Development Community (SADC) for providing the Tanzania aeromagnetic data used in this study. This is the Oklahoma State University Boone Pickens School of Geology contribution no. 2018-.

References

Baer, G., 1991. Mechanisms of dike propagation in layered rocks and in massive, porous sedimentary rocks. *Journal of Geophysical Research: Solid Earth*, *96*(B7), pp.11911-11929.

Baranov, V., 1957. A new method for interpretation of aeromagnetic maps: pseudo-gravimetric anomalies. *Geophysics*, *22*(2), pp.359-382.

Boniface, N. and Schenk, V., 2012. Neoproterozoic eclogites in the Paleoproterozoic Ubendian belt of Tanzania: Evidence for a Pan-African suture between the Bangweulu block and the Tanzania craton. *Precambrian Research*, *208*, pp.72-89.

Boniface, N., Schenk, V. and Appel, P., 2012. Paleoproterozoic eclogites of MORB-type chemistry and three Proterozoic orogenic cycles in the Ubendian Belt (Tanzania): Evidence from monazite and zircon geochronology, and geochemistry. *Precambrian Research*, *192*, pp.16-33.

Borrego, D.J., 2016. Crustal Structure of the Rungwe Volcanic Province and Region Surrounding the Northern Lake Malawi Rift Basin. MSc Thesis, Pennsylvania State University.

Bosworth, W., 1985. Geometry of propagating continental rifts. *Nature*, *316*(6029), p.625.

Boven, A., Theunissen, K., Sklyarov, E., Klerkx, J., Melnikov, A., Mruma, A. and Punzalan, L., 1999. Timing of exhumation of a high-pressure mafic granulite terrane of the Paleoproterozoic Ubende belt (West Tanzania). *Precambrian Research*, *93*(1), pp.119-137.

Brune, S. and Autin, J., 2013. The rift to break-up evolution of the Gulf of Aden: Insights from 3D numerical lithospheric-scale modelling. *Tectonophysics*, *607*, pp.65-79.

878 Brune, S., Corti, G. and Ranalli, G., 2017. Controls of inherited lithospheric heterogeneity on rift
879 linkage: Numerical and analog models of interaction between the Kenyan and Ethiopian
880 rifts across the Turkana depression. *Tectonics, 36*(9), pp.1767-1786.
881 Camelbeeck, T. and Iranga, M.D., 1996. Deep crustal earthquakes and active faults along the
882 Rukwa trough, eastern Africa. *Geophysical Journal International, 124*(2), pp.612-630.
883 Castaing, C., 1991. Post-Pan-African tectonic evolution of South Malawi in relation to the
884 Karroo and recent East African rift systems. *Tectonophysics, 191*(1-2), pp.55-73.
885 Chorowicz, J., 1989. Transfer and transform fault zones in continental rifts: examples in the
886 Afro-Arabian rift system. Implications of crust breaking. *Journal of African Earth*
887 *Sciences (and the Middle East), 8(2-4)*, pp.203-214.
888 Chorowicz, J., 2005. The east African rift system. *Journal of African Earth Sciences*, *43*(1),
889 pp.379-410.
890 Collanega, L., Bell, R., Coleman, A.J., Lenhart, A. and Breda, A., 2018. How do intra-basement
891 fabrics influence normal fault growth? Insights from the Taranaki Basin, offshore New
892 Zealand. EarthArxiv, DOI: 10.31223/osf.io/8rn9u
893 Corti, G., 2012. Evolution and characteristics of continental rifting: Analog modeling-inspired
894 view and comparison with examples from the East African Rift System. *Tectonophysics,*
895 *522*, pp.1-33.
896 Daly, M.C., 1988. Crustal Shear Zones in Central Africa - A kinematic approach to Proterozoic
897 Tectonics. *Episodes*, *11*(1), pp.5-11.
898 Daly, M.C., Chorowicz, J. and Fairhead, J.D., 1989. Rift basin evolution in Africa: the influence
899 of reactivated steep basement shear zones. *Geological Society, London, Special*
900 *Publications, 44*(1), pp.309-334.

Dawson, S.M., Laó-Dávila, D.A., Atekwana, E.A. and Abdelsalam, M.G., 2018. The influence of the Precambrian Mughese Shear Zone structures on strain accommodation in the northern Malawi Rift. *Tectonophysics*, *722*, pp.53-68.

Delvaux, D., and Hanon, M., 1991. Neotectonics of the Mbeya area, SW Tanzania. *Annual report of the Royal Museum of Central Africa, Department of Geology and Mineralogy, 1992*, pp.87-97.

Delvaux, D., Kervyn, F., Macheyeki, A.S. and Temu, E.B., 2012. Geodynamic significance of the TRM segment in the East African Rift (W-Tanzania): Active tectonics and paleostress in the Ufipa plateau and Rukwa basin. *Journal of Structural Geology*, *37*, pp.161-180.

Delvaux, D., Levi, K., Kajara, R. and Sarota, J., 1992. Cenozoic paleostress and kinematic evolution of the Rukwa–North Malawi rift valley (East African Rift System). *Bulletin des Centres de Recherche Exploration-Production ElfAquitaine*, *16*, pp.383-406.

Fernandez-Alonso, M., Delvaux, D., Klerkx, J. and Theunissen, K., 2001. Structural link between Tanganyika-and Rukwa-rift basins at Karema-Nkamba (Tanzania): basement structural control and recent evolution. *Mus. Roy. Afr. Centr., Tervuren (Belgique), Dép. Géol. Min., Rap. Ann*, pp.91-100.

Fontijn, K., Delvaux, D., Ernst, G.G., Kervyn, M., Mbede, E. and Jacobs, P., 2010. Tectonic control over active volcanism at a range of scales: case of the Rungwe Volcanic Province, SW Tanzania; and hazard implications. *Journal of African Earth Sciences*, *58*(5), pp.764-777.

Fontijn, K., Williamson, D., Mbede, E. and Ernst, G.G., 2012. The Rungwe Volcanic Province, Tanzania–A volcanological review. *Journal of African Earth Sciences*, *63*, pp.12-31.

Fossen, H., 2010. *Structural geology*. Cambridge University Press.

924 Fossen, H. and Rotevatn, A., 2016. Fault linkage and relay structures in extensional settings—A
925 review. *Earth-Science Reviews, 154*, pp.14-28.
926 Foster, A., Ebinger, C., Mbede, E. and Rex, D., 1997. Tectonic development of the northern
927 Tanzanian sector of the East African Rift System. *Journal of the Geological*
928 *Society, 154*(4), pp.689-700.
929 Fritz, H., Abdelsalam, M., Ali, K.A., Bingen, B., Collins, A.S., Fowler, A.R., Ghebreab, W.,
930 Hauzenberger, C.A., Johnson, P.R., Kusky, T.M. and Macey, P., 2013. Orogen styles in
931 the East African Orogen: a review of the Neoproterozoic to Cambrian tectonic
932 evolution. *Journal of African Earth Sciences, 86*, pp.65-106.
933 Gawthorpe, R.L., Jackson, C.A.L., Young, M.J., Sharp, I.R., Moustafa, A.R. and Leppard, C.W.,
934 2003. Normal fault growth, displacement localisation and the evolution of normal fault
935 populations: the Hammam Faraun fault block, Suez rift, Egypt. *Journal of Structural*
936 *Geology, 25*(6), 883-895.
937 Grauch, V.J.S. and Hudson, M.R., 2007. Guides to understanding the aeromagnetic expression of
938 faults in sedimentary basins: Lessons learned from the central Rio Grande rift, New
939 Mexico. *Geosphere, 3*(6), pp.596-623.
940 Grauch, V.J.S. and Hudson, M.R., 2011. Aeromagnetic anomalies over faulted strata. *The*
941 *Leading Edge, 30*(11), pp.1242-1252.
942 Gudmundsson, A. and Brenner, S.L., 2001. How hydrofractures become arrested. *Terra*
943 *Nova, 13*(6), pp.456-462.
944 Hayward, N.J. and Ebinger, C.J., 1996. Variations in the along-axis segmentation of the Afar
945 Rift system. *Tectonics, 15*(2), pp.244-257.

946 Helgeson, D.E. and Aydin, A., 1991. Characteristics of joint propagation across layer interfaces
947 in sedimentary rocks. *Journal of Structural Geology*, *13*(8), pp.897-911.
948 Henderson, R.G. and Zietz, I., 1949. The upward continuation of anomalies in total magnetic
949 intensity fields. *Geophysics*, *14*(4), pp. 517-534.
950 Hodge, M., Fagereng, Å., Biggs, J., and Mdala, H., 2018.. Controls on early-rift geometry: New
951 perspectives from the Bilila-Mtakataka fault, Malawi. *Geophysical Research Letters, 45*,
952 3896–3905.
953 Hodgson, I., Illsley-Kemp, F., Gallacher, R.J., Keir, D., Ebinger, C.J. and Mtelela, K., 2017.
954 Crustal structure at a young continental rift: A receiver function study from the
955 Tanganyika Rift. *Tectonics*, *36*(12), pp.2806-2822.
956 Jackson, J. and Blenkinsop, T., 1997. The Bilila-Mtakataka fault in Malaŵi: An active, 100-km
957 long, normal fault segment in thick seismogenic crust. *Tectonics*, *16*(1), pp.137-150.
958 Johnson, S., Mendez, K., Beresh, S.C.M., Mynatt, W.G., Elifritz, E.A., Laó-Dávila, D.A.,
959 Atekwana, E.A., Abdelsalam, M.G., Chindandali, P.R.N., Chisenga, C. and Gondwe, S.,
960 2017.. The Relationships of Subparallel Synthetic Faults and Pre-existing Structures in
961 the Central Malawi Rift. *AGU Fall Meeting poster number T22C-03*.
962 Katumwehe, A.B., Abdelsalam, M.G. and Atekwana, E.A., 2015. The role of pre-existing
963 Precambrian structures in rift evolution: The Albertine and Rhino grabens,
964 Uganda. *Tectonophysics*, *646*, pp.117-129.
965 Kervyn, F., Ayub, S., Kajara, R., Kanza, E. and Temu, B., 2006. Evidence of recent faulting in
966 the Rukwa rift (West Tanzania) based on radar interferometric DEMs. *Journal of African*
967 *Earth Sciences*, *44*(2), pp.151-168.

968 Kilembe, E.A. and Rosendahl, B.R., 1992. Structure and stratigraphy of the Rukwa
969 rift. *Tectonophysics*, *209*(1-4), pp.143-158.
970 Kim, S., Nyblade, A.A. and Baag, C.E., 2009. Crustal velocity structure of the Rukwa Rift in the
971 western branch of the East African Rift system. *South African Journal of Geology*, *112*(3-
972 4), pp.251-260.
973 Kinabo, B.D., Atekwana, E.A., Hogan, J.P., Modisi, M.P., Wheaton, D.D. and Kampunzu, A.B.,
974 2007. Early structural development of the Okavango rift zone, NW Botswana. *Journal of*
975 *African Earth Sciences*, *48*(2), pp.125-136.
976 Kinabo, B.D., Hogan, J.P., Atekwana, E.A., Abdelsalam, M.G. and Modisi, M.P., 2008. Fault
977 growth and propagation during incipient continental rifting: Insights from a combined
978 aeromagnetic and Shuttle Radar Topography Mission digital elevation model
979 investigation of the Okavango Rift Zone, northwest Botswana. *Tectonics*, *27*(3).
980 Koehn, D., Aanyu, K., Haines, S. and Sachau, T., 2008. Rift nucleation, rift propagation and the
981 creation of basement micro-plates within active rifts. *Tectonophysics*, *458*(1-4), pp.105-
982 116.
983 Kolawole, F., Atekwana, E.A., Laó-Dávila, D.A., Abdelsalam, M.G., Chindandali, P.R., Salima,
984 J. and Kalindekafe, L., 2018. Active deformation of Malawi Rift's North Basin hinge
985 zone modulated by reactivation of pre-existing Precambrian shear zone fabric. *Tectonics*,
986 *37*, pp.683–704.
987 Lao-Davila, D.A., Al-Salmi, H.S., Abdelsalam, M.G. and Atekwana, E.A., 2015. Hierarchical
988 segmentation of the Malawi Rift: The influence of inherited lithospheric heterogeneity
989 and kinematics in the evolution of continental rifts. *Tectonics*, *34*(12), pp.2399-2417.

990 Lawley, C.J., Selby, D., Condon, D.J., Horstwood, M., Millar, I., Crowley, Q. and Imber, J.,
991 2013. Lithogeochemistry, geochronology and geodynamic setting of the Lupa Terrane,
992 Tanzania: implications for the extent of the Archean Tanzanian Craton. *Precambrian*
993 *Research, 231*, pp.174-193.
994 Lenoir, J.L., Liégeois, J.P., Theunissen, K. and Klerkx, J., 1994. The Palaeoproterozoic
995 Ubendian shear belt in Tanzania: geochronology and structure. *Journal of African Earth*
996 *Sciences, 19*(3), pp.169-184.
997 Mbede, E.I., 2002. Interpretation of refelction seismic data from the Usangu Basin, East African
998 Rift System. *Tanzania Journal of Science, 28*(1), pp.83-97.
999 McCalpin, J.P., Rockwell, T.K. and Weldon II, R.J., 2009. Paleoseismology of Strike-Slip
1000 Tectonic Environments. *International Geophysics, 95*, pp.421-496.
1001 Modisi, M.P., Atekwana, E.A., Kampunzu, A.B. and Ngwisanyi, T.H., 2000. Rift kinematics
1002 during the incipient stages of continental extension: Evidence from the nascent Okavango
1003 rift basin, northwest Botswana. *Geology, 28*(10), pp.939-942.
1004 Morley, C.K., 1995. Developments in the structural geology of rifts over the last decade and their
1005 impact on hydrocarbon exploration. *Geological Society, London, Special*
1006 *Publications, 80*(1), pp.1-32.
1007 Morley, C.K., 2010. Stress re-orientation along zones of weak fabrics in rifts: An explanation
1008 for pure extension in 'oblique' rift segments?. *Earth and Planetary Science*
1009 *Letters*, *297*(3), pp.667-673.
1010 Morley, C.K., Cunningham, S.M., Harper, R.M. and Wescott, W.A., 1992. Geology and
1011 geophysics of the Rukwa rift, East Africa. *Tectonics, 11*(1), pp.69-81.

1012 Morley, C.K., Nelson, R.A., Patton, T.L. and Munn, S.G., 1990. Transfer zones in the East
1013 African rift system and their relevance to hydrocarbon exploration in rifts (1). *AAPG*
1014 *Bulletin*, *74*(8), pp.1234-1253.
1015 Mortimer, E., Paton, D.A., Scholz, C.A., Strecker, M.R. and Blisniuk, P., 2007. Orthogonal to
1016 oblique rifting: effect of rift basin orientation in the evolution of the North basin, Malawi
1017 Rift, East Africa. *Basin Research*, *19*(3), pp.393-407.
1018 Muirhead, J.D. and Kattenhorn, S.A., 2018. Activation of preexisting transverse structures in an
1019 evolving magmatic rift in East Africa. *Journal of Structural Geology, 106*, pp.1-18.
1020 Njinju, E.A., Atekwana, E.A., Stamps, D.S., Abdelsalam, M.G., Atekwana, E.A., Mickus, K.L.,
1021 Kolawole, F. and Nyalugwe, V., 2018. Lithospheric Structure of the Malawi Rift:
1022 Implications for Rifting Processes in Magma Poor Rift Systems. *EarthArXiv*, DOI:
1023 10.31223/osf.io/83qd9
1024 Peirce, J.W. and Lipkov, L., 1988. Structural interpretation of the Rukwa rift, Tanzania.
1025 *Geophysics*, *53*(6), pp.824-836.
1026 Phillips, T.B., Jackson, C.A., Bell, R.E., Duffy, O.B. and Fossen, H., 2016. Reactivation of
1027 intrabasement structures during rifting: A case study from offshore southern
1028 Norway. *Journal of Structural Geology*, *91*, pp.54-73.
1029 Pik, R., Marty, B., Carignan, J., Yirgu, G. and Ayalew, T., 2008. Timing of East African Rift
1030 development in southern Ethiopia: Implication for mantle plume activity and evolution of
1031 topography. *Geology*, *36*(2), pp.167-170.
1032 Ring, U., Kröner, A., Buchwaldt, R., Toulkeridis, T. and Layer, P.W., 2002. Shear-zone patterns
1033 and eclogite-facies metamorphism in the Mozambique belt of northern Malawi, east-

central Africa: implications for the assembly of Gondwana. *Precambrian Research*, *116*(1), pp.19-56.

Rosendahl, B.R., 1987. Architecture of continental rifts with special reference to East Africa. *Annual Review of Earth and Planetary Sciences*, *15*(1), pp.445-503.

Rotevatn, A., Jackson, C.A.L., Tvedt, A.B.M., Bell, R. and Blækkan, I., 2018. How do normal faults grow?. EarthArXiv.

Salem, A., Williams, S., Fairhead, J.D., Ravat, D. and Smith, R., 2007. Tilt-depth method: A simple depth estimation method using first-order magnetic derivatives. *The Leading Edge*, *26*(12), pp.1502-1505.

Sarafian, E., Evans, R.L., Abdelsalam, M.G., Atekwana, E., Elsenbeck, J., Jones, A.G. and Chikambwe, E., 2018. Imaging Precambrian lithospheric structure in Zambia using electromagnetic methods. *Gondwana Research*, *54*, pp.38-49.

Scholz, C.H. and Contreras, J.C., 1998. Mechanics of continental rift architecture. *Geology*, *26*(11), pp.967-970.

Silva, J.B., 1986. Reduction to the pole as an inverse problem and its application to low-latitude anomalies. *Geophysics*, *51*(2), pp.369-382.

Siuda, K., Magee, C., Bell, R., Jackson, C.A.L. and Collanega, L., 2018. Pre-existing basement thrusts influence rifting in the Taranaki Basin, New Zealand. EarthArXiv.

Szatmari, P. and Milani, E.J., 1999. Microplate rotation in northeast Brazil during South Atlantic rifting: Analogies with the Sinai microplate. *Geology*, *27*(12), pp.1115-1118.

Taylor, B., Weiss, J.R., Goodliffe, A.M., Sachpazi, M., Laigle, M. and Hirn, A., 2011. The structures, stratigraphy and evolution of the Gulf of Corinth rift, Greece. *Geophysical Journal International*, *185*(3), pp.1189-1219.

1057 Theunissen, K., Klerkx, J., Melnikov, A. and Mruma, A., 1996. Mechanisms of inheritance of
1058 rift faulting in the western branch of the East African Rift, Tanzania. *Tectonics, 15*(4),
1059 pp.776-790.
1060 Van de Velde, P., and De Waele, B., 1998. Geology of the Mupamadzi River area. Explanation
1061 of degree sheet 1231, SW quarter, Report No. 105, *Geological Survey Department,*
1062 *Republic of Zambia.*
1063 Versfelt, J. and Rosendahl, B.R., 1989. Relationships between pre-rift structure and rift
1064 architecture in Lakes Tanganyika and Malawi, East Africa. *Nature, 337*(6205), p.354.
1065 Wheeler, W.H. and Karson, J.A., 1989. Structure and kinematics of the Livingstone Mountains
1066 border fault zone, Nyasa (Malawi) Rift, southwestern Tanzania. *Journal of African Earth*
1067 *Sciences (and the Middle East)*, *8*(2-4), pp.393-413.
1068 Wheeler, W.H. and Karson, J.A., 1994. Extension and subsidence adjacent to a "weak"
1069 continental transform: An example from the Rukwa rift, East Africa. *Geology*, *22*(7),
1070 pp.625-628.
1071 Wichura, H., Bousquet, R., Oberhänsli, R., Strecker, M.R. and Trauth, M.H., 2011. The Mid-
1072 Miocene East African Plateau: a pre-rift topographic model inferred from the
1073 emplacement of the phonolitic Yatta lava flow, Kenya. *Geological Society, London,*
1074 *Special Publications, 357*(1), pp.285-300.
1075 Wilson, T.J., 1999. Cenozoic structural segmentation of the Transantarctic Mountains rift flank
1076 in southern Victoria Land. *Global and Planetary Change*, *23*(1-4), pp.105-127.
1077 Wu, D. and Bruhn, R.L., 1994. Geometry and kinematics of active normal faults, South Oquirrh
1078 Mountains, Utah: implication for fault growth. *Journal of Structural Geology, 16*(8),
1079 pp.1061-1075.

Xue, L., Gani, N.D. and Abdelsalam, M.G., 2017. Geomorphologic proxies for bedrock rivers: A case study from the Rwenzori Mountains, East African Rift system. *Geomorphology, 285*, pp.374-398.

Zhang, X. and Jeffrey, R.G., 2008. Reinitiation or termination of fluid-driven fractures at frictional bedding interfaces. *Journal of Geophysical Research: Solid Earth*, *113*(B8).

Zhang, X., Jeffrey, R.G. and Thiercelin, M., 2007. Deflection and propagation of fluid-driven fractures at frictional bedding interfaces: a numerical investigation. *Journal of Structural Geology*, *29*(3), pp.396-410.

Zhao, M., Langston, C.A., Nyblade, A.A. and Owens, T.J., 1997. Lower-crustal rifting in the Rukwa graben, East Africa. *Geophysical Journal International*, *129*(2), pp.412-420.

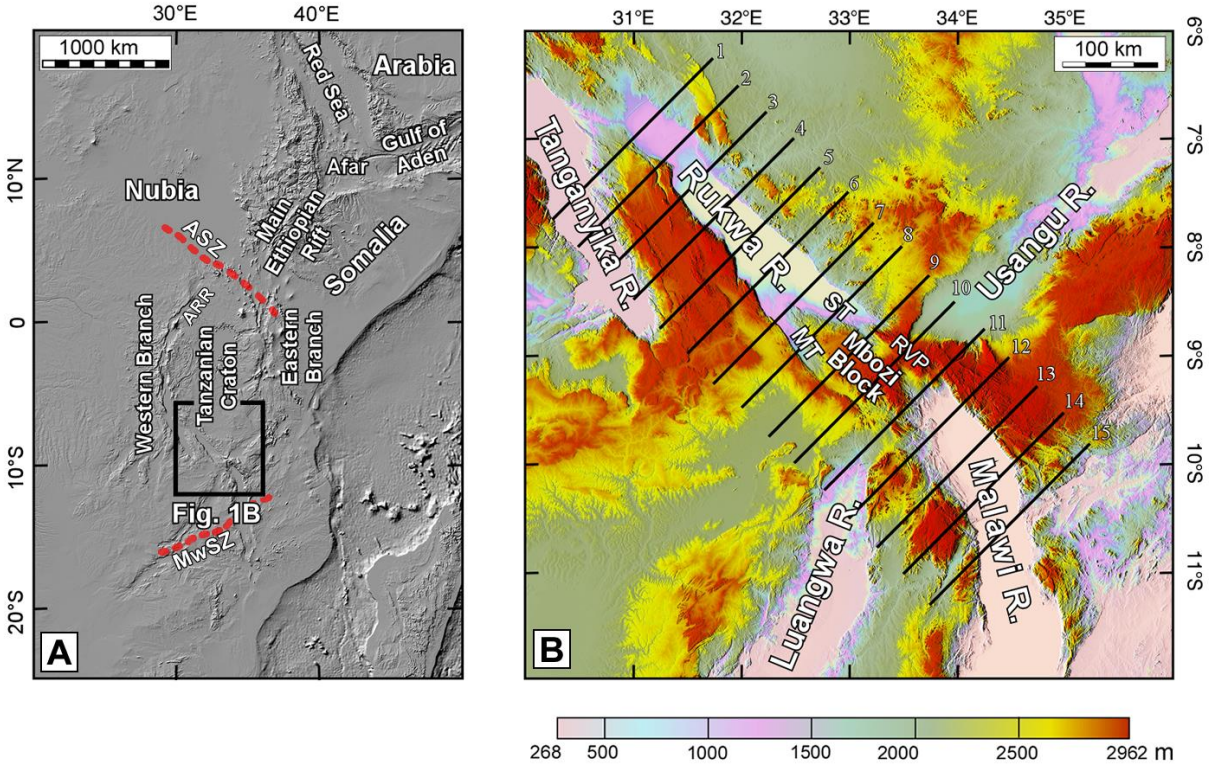

Fig.1. (A) Topographic map of the East African Rift System, showing the segments of the rift system and the location of the Rukwa-North Malawi Rift Segment (RNMRS) (black square). (B) Digital Elevation Model (DEM) of the RNMRS showing the different domains. Solid black lines represent topographic profile lines shown in Figure 3. ARR= Albertine-Rhino Rift, ASZ= Aswa Shear Zone, MT= Musangano Trough, MwSZ= Mwembeshi Shear Zone, RVP= Rungwe Volcanic Province, ST= Songwe Trough.

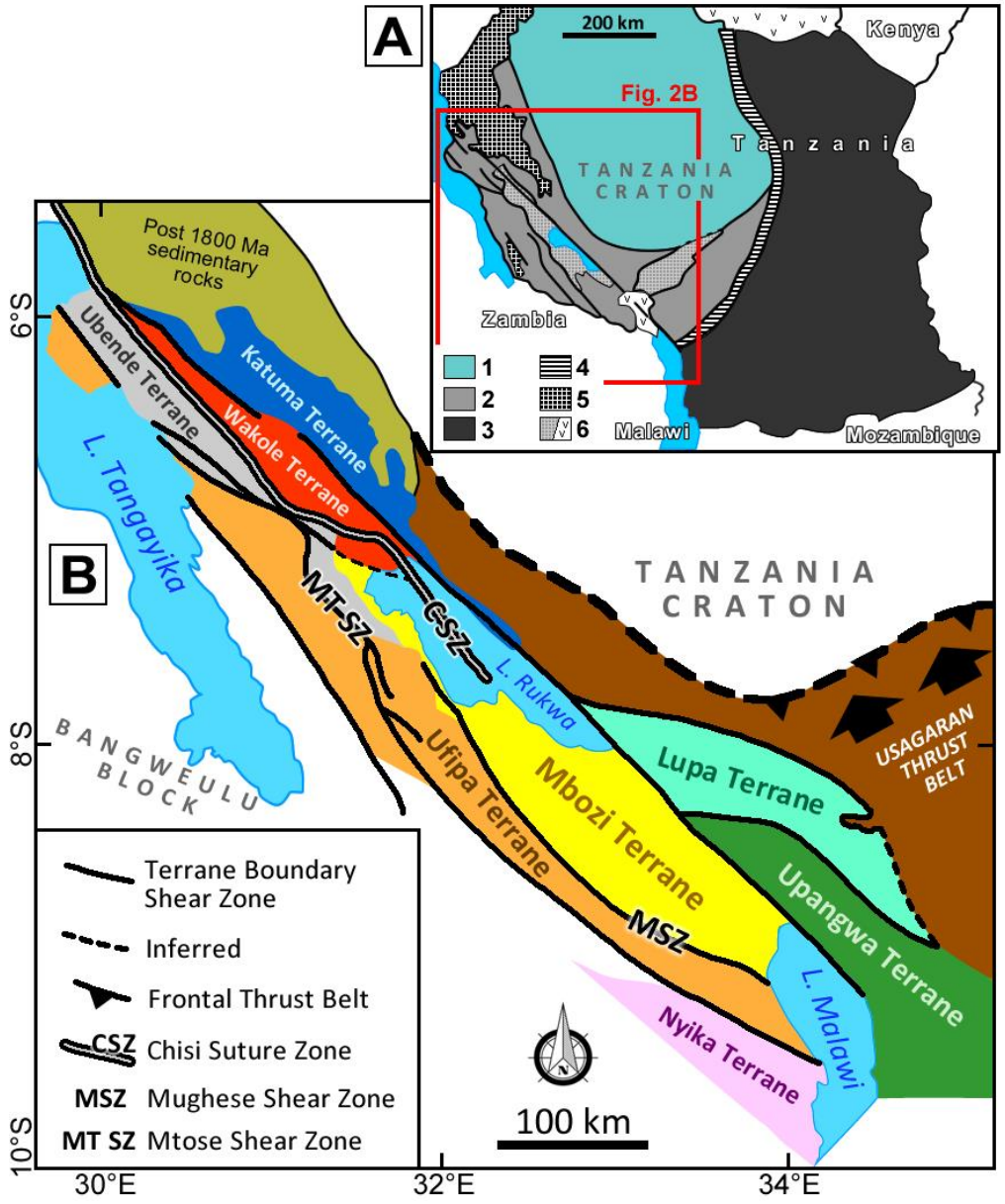

Fig. 2. (A) Precambrian domains around the Tanzanian Craton (modified after Theunissen et al., 1996; Boven et al., 1999; Fernandez-Alonso et al., 2001; Schenk et al., 2006). 1 = Archean craton; 2 = Paleoproterozoic Usagaran and Ubendian orogenic belts; 3 = Mozambique orogenic belt; 4 = western limit of Pan-African influence; 5 = Meso and/or Neoproterozoic sediments *(only for the Ubendian Belt region)*; 6 = Phanerozoic volcanics and sedimentary rocks. (B) Regional geological map of southwest Tanzania showing the terrane structure of the Ubendian orogenic belt within which the Rukwa-Malawi Rift Segment (RNMRS) developed.

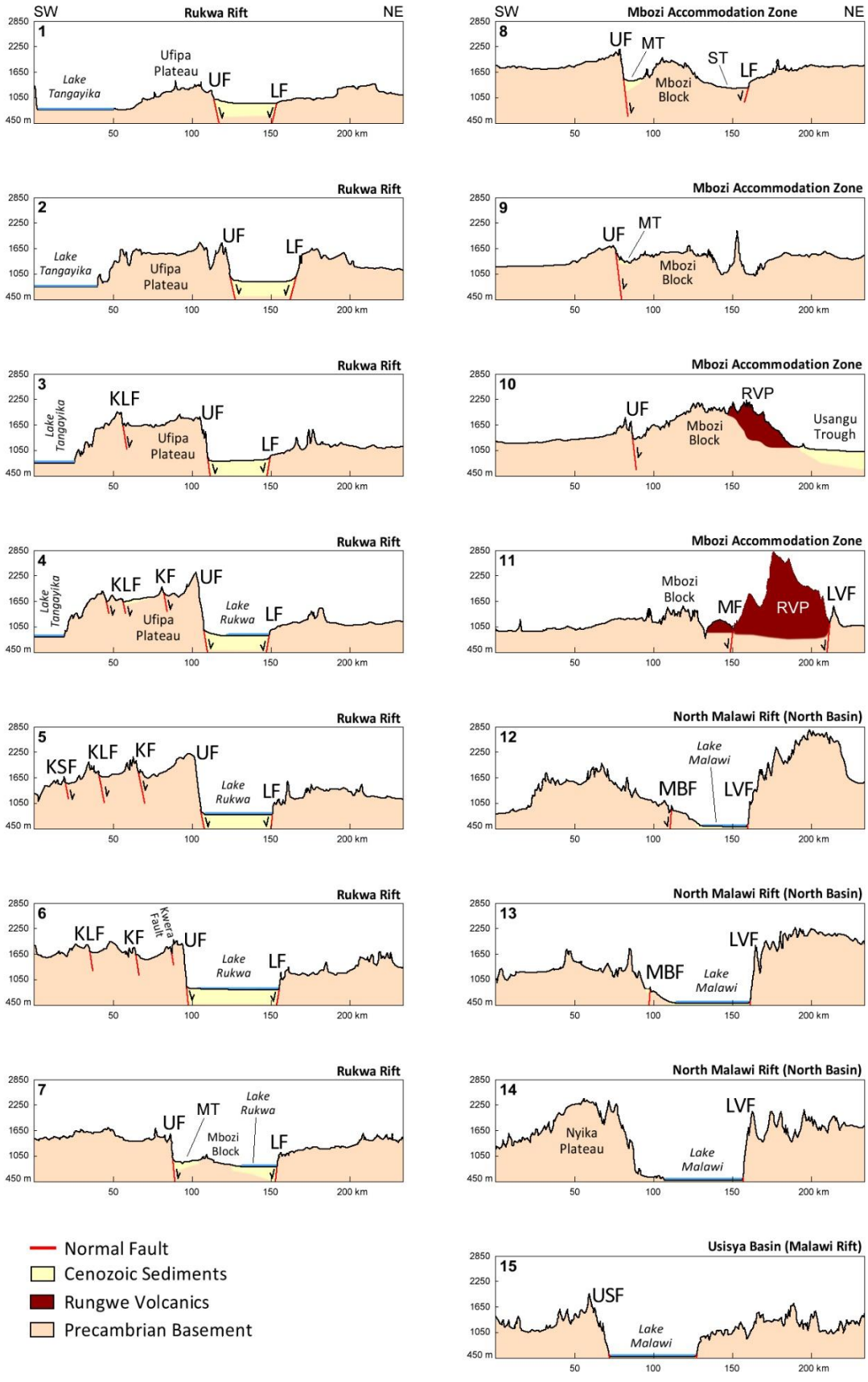
SW
Rukwa Rift
NE
1
Lake Tangayika
Ufipa Plateau
UF
LF
2
KLF
3
KF
4
KSF
5
Kwera Fault
6
MT
7
Mbozi Block
Lake Rukwa
Mbozi Accommodation Zone
8
ST
9
10
RVP
Usangu Trough
11
MF
LVF
North Malawi Rift (North Basin)
12
Lake Malawi
MBF
13
14
Nyika Plateau
Usisya Basin (Malawi Rift)
15
USF
2850
2250
1650
1050
450 m
50
100
150
200 km
Normal Fault
Cenozoic Sediments
Rungwe Volcanics
Precambrian Basement

Fig. 3. Topographic profiles across the Rukwa - North Malawi Rift segment. Profile numbers correspond to the profiles in Figure 1B. KLF = Kalambo Fault, KF = Kanda Fault, KSF = Kasanga Fault, LF = Lupa Fault, LVF = Livingstone Fault, MB = Mbozi Block, MBF = Mbiri Fault, MF = Mbaka Fault, MT = Musangano Trough, RVP = Rungwe Volcanic Province, ST = Songwe Trough, UF = Ufipa Fault, USF = Usisya Fault.

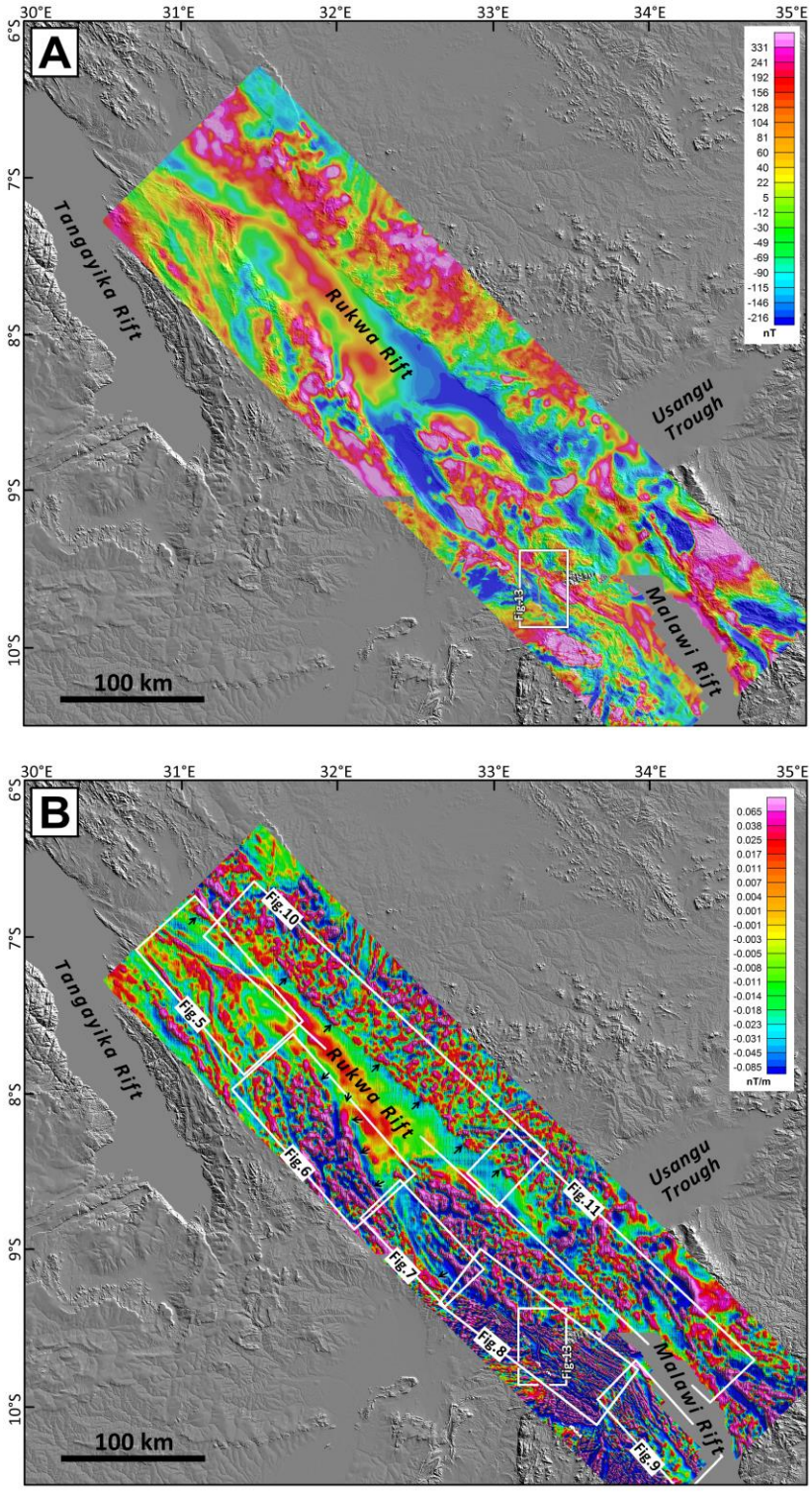

Fig. 4. (A) The reduced to pole Total Magnetic Intensity (RTP-TMI) map of the Rukwa-North Malawi Rift area, draped over the topographic digital elevation model of SW Tanzania. (B) The 1st vertical derivative map of the RTP-TMI map of the Rukwa-North Malawi Rift area draped over the topographic digital elevation model.

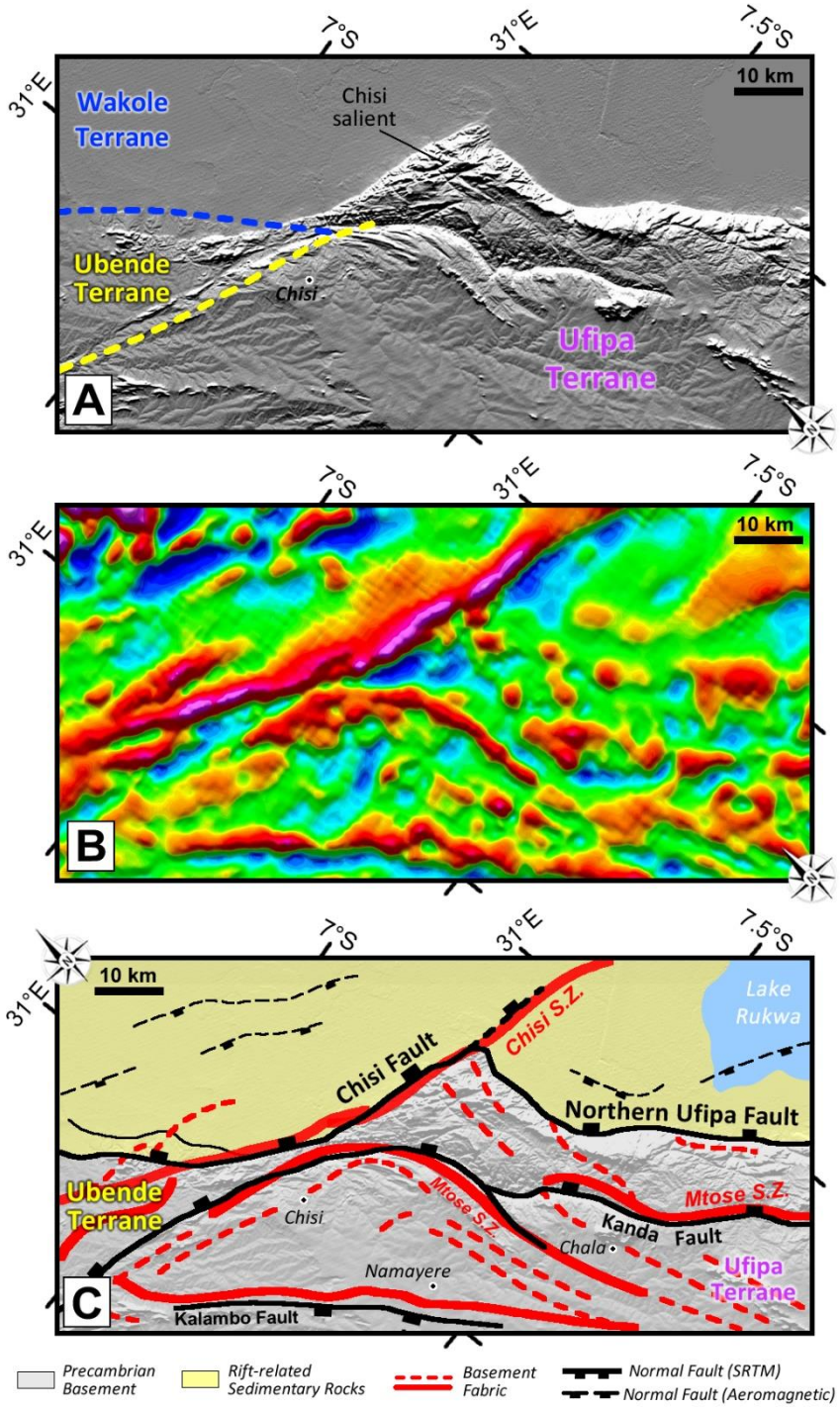

Fig. 5. Northernmost part of the Ufipa Fault, the SW boundary fault of the Rukwa Rift. Topographic digital elevation model in the top panel (A), the vertical derivative of the magnetic data in the middle panel (B), and a structural interpretation in the bottom panel (C).

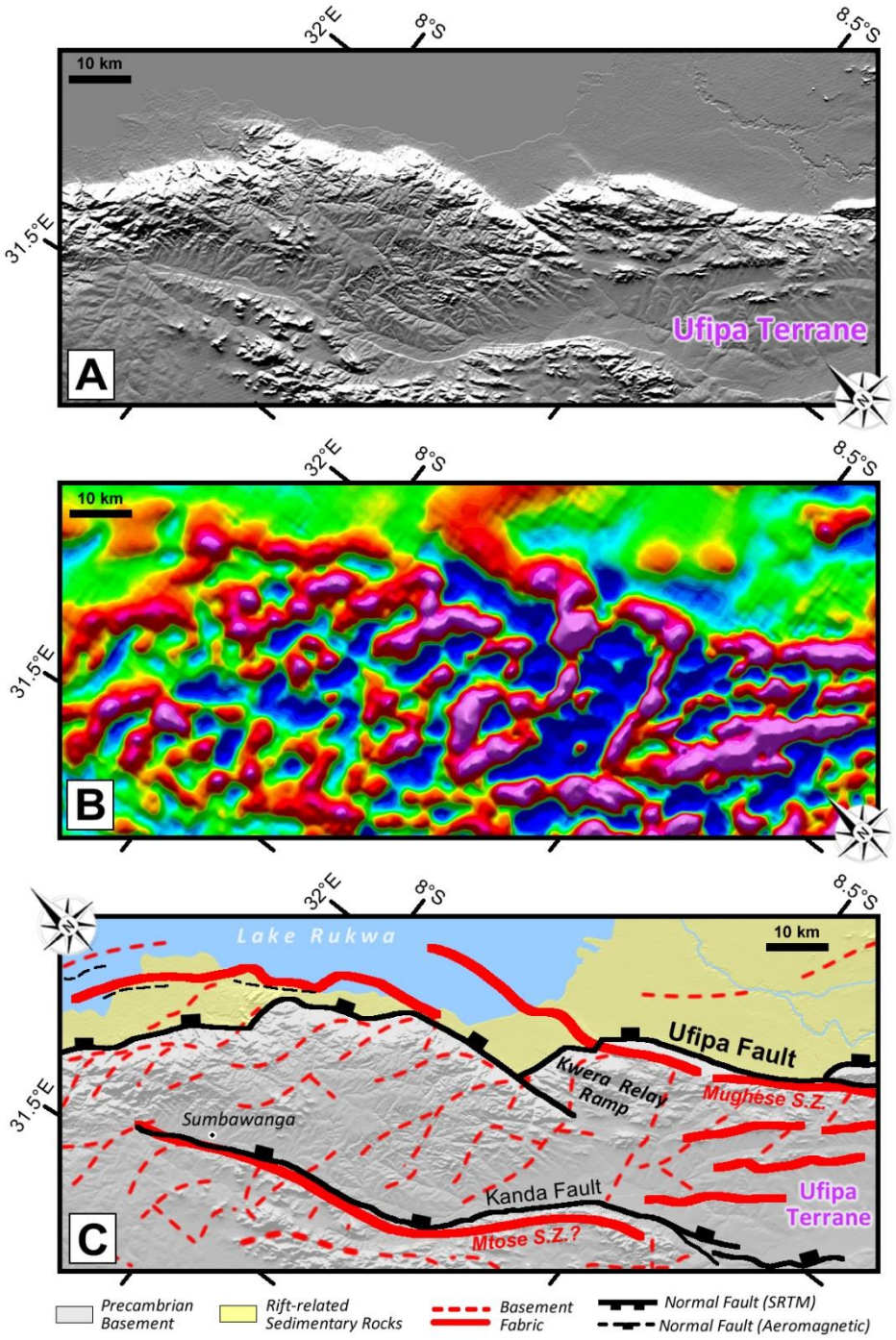

Fig. 6. Central segment of the Ufipa Fault, SW boundary of the Rukwa Rift. Topographic digital elevation model in the top panel (A), the vertical derivative of the magnetic data in the middle panel (B), and a structural interpretation in the bottom panel (C).

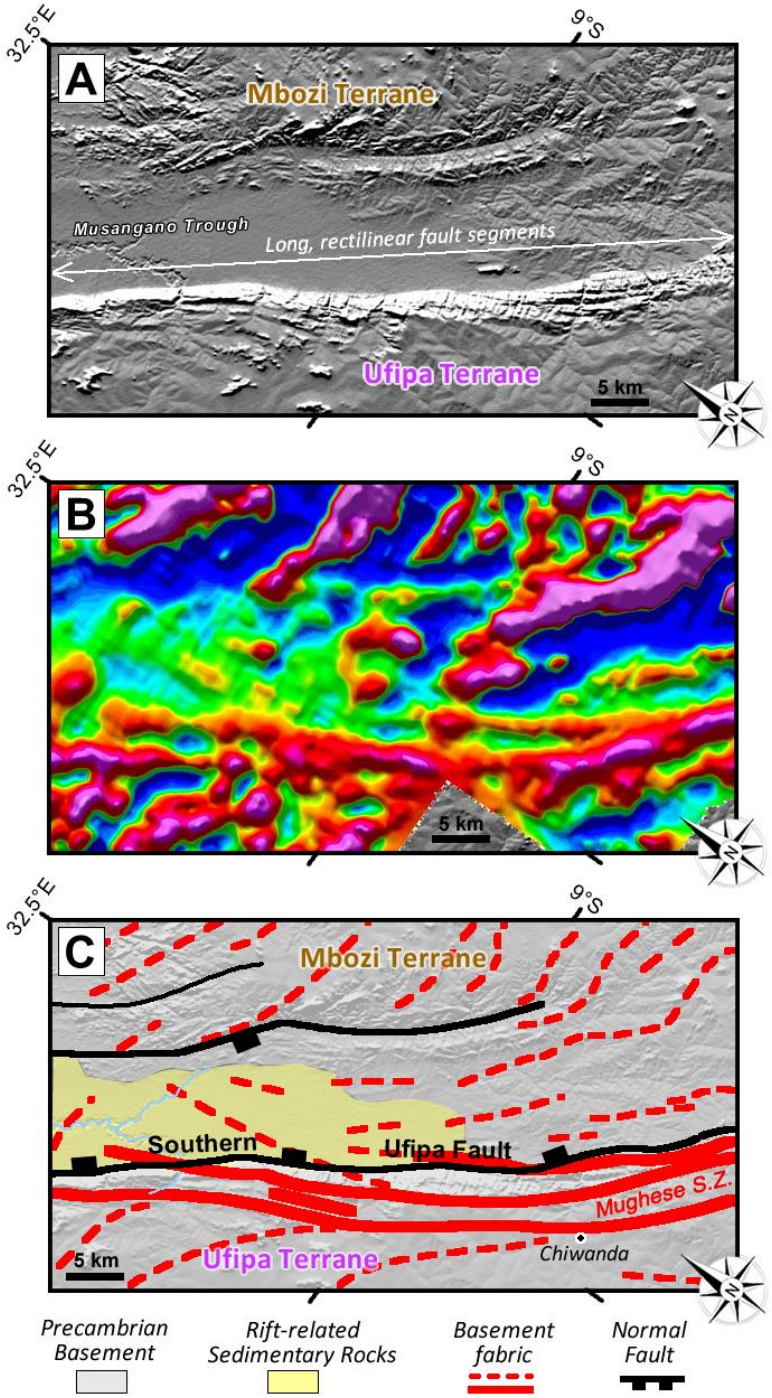

Fig. 7. The Musangano Trough part of the SW boundary of the Rukwa Rift. Topographic digital elevation model in the top panel (A), the vertical derivative of the magnetic data in the middle panel (B), and a structural interpretation in the bottom panel (C).

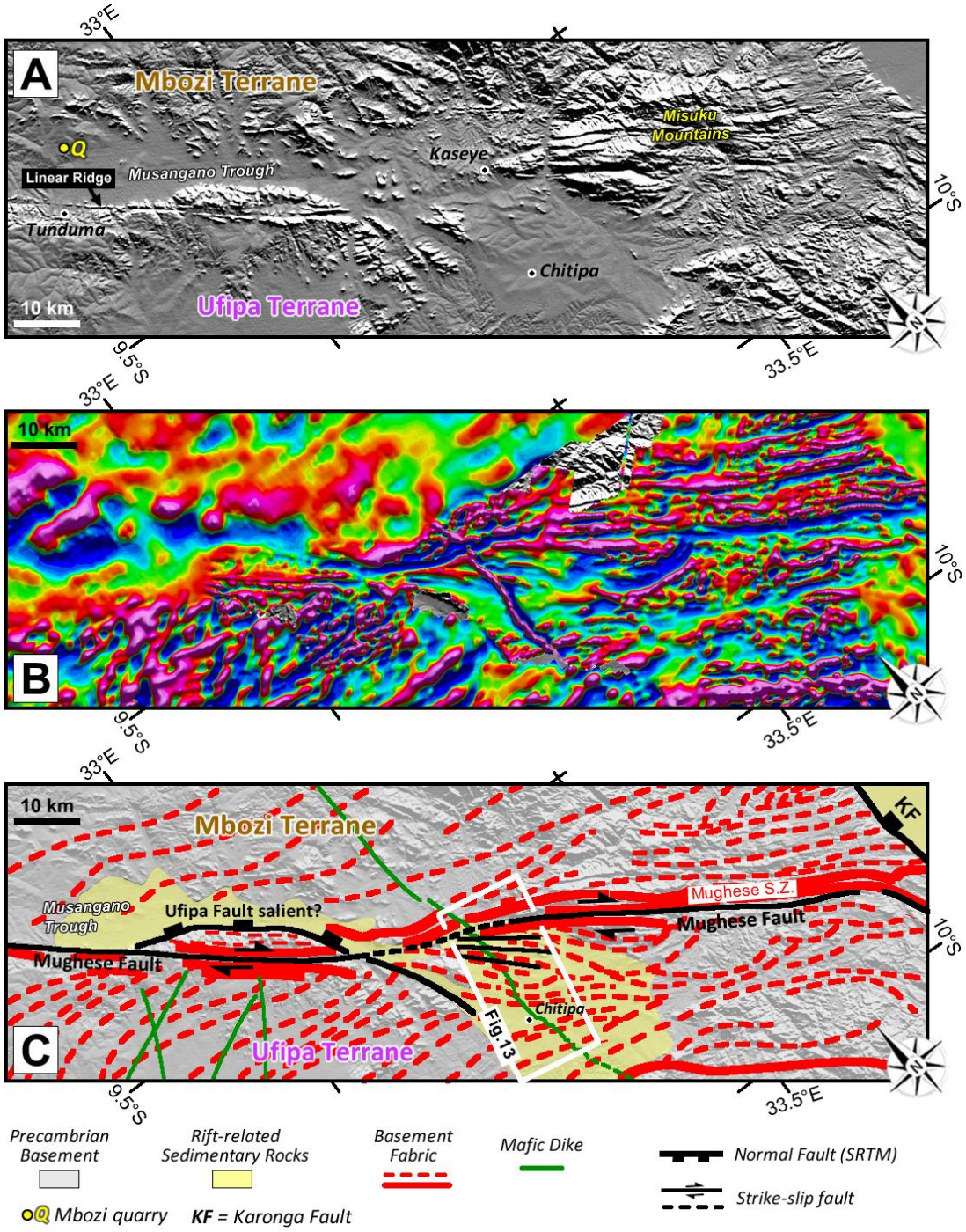

Fig. 8. The SW margin of the Mbozi Block. Topographic digital elevation model in the top panel (A), the vertical derivative of the magnetic data in the middle panel (B), and a structural interpretation in the bottom panel (C).

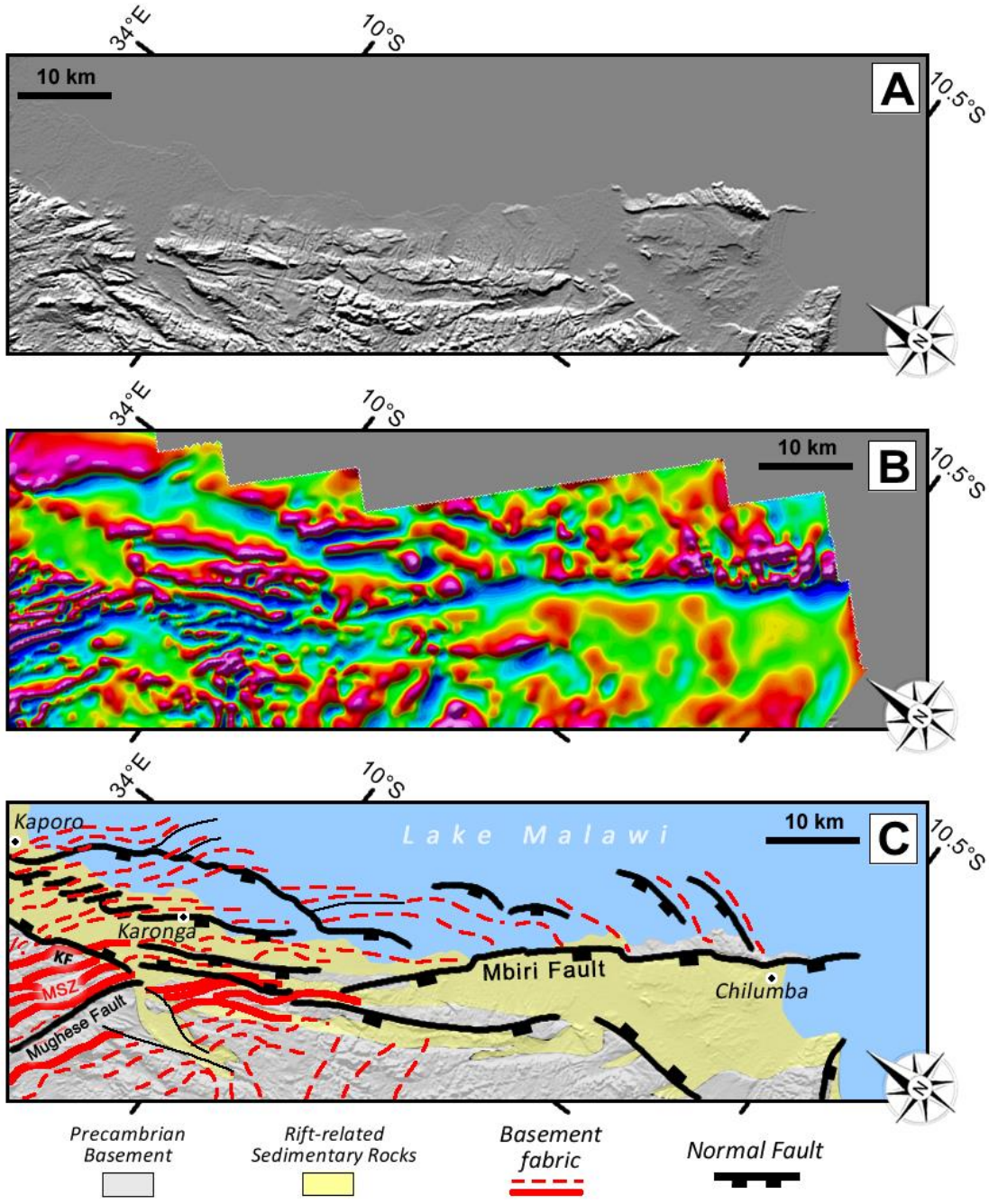

Fig. 9. The SW margin of the North Malawi Rift Basin (Karonga area). Topographic digital elevation model in the top panel (A), the vertical derivative of the magnetic data in the middle panel (B), and a structural interpretation in the bottom panel (C). MSZ = Mughese Shear Zone, KF = Karonga Fault. Fault and basement fabric interpretations from Kolawole et al. (2018).

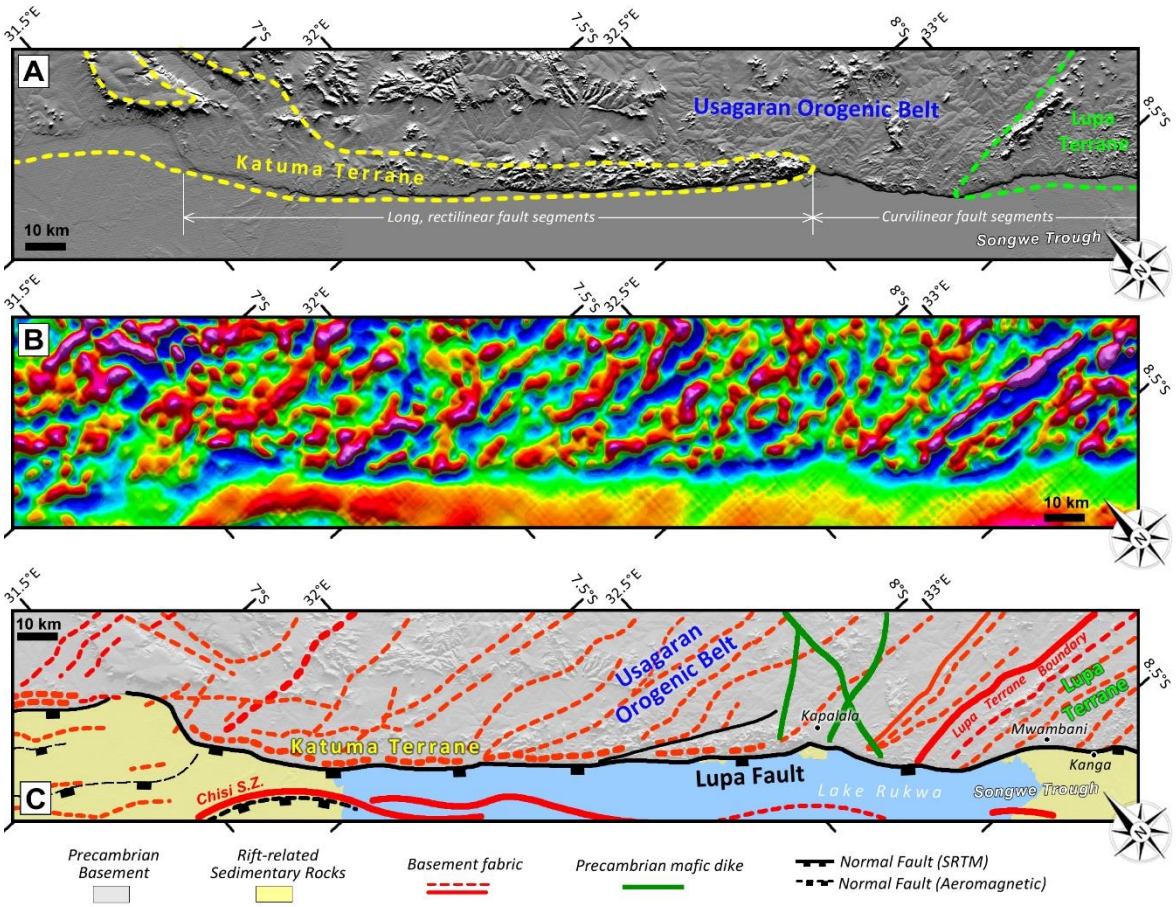

Fig. 10. The northern section of the Lupa Fault, the NE boundary fault of the Rukwa Rift. Topographic digital elevation model in the top panel (A), the vertical derivative of the magnetic data in the middle panel (B), and a structural interpretation in the bottom panel (C).

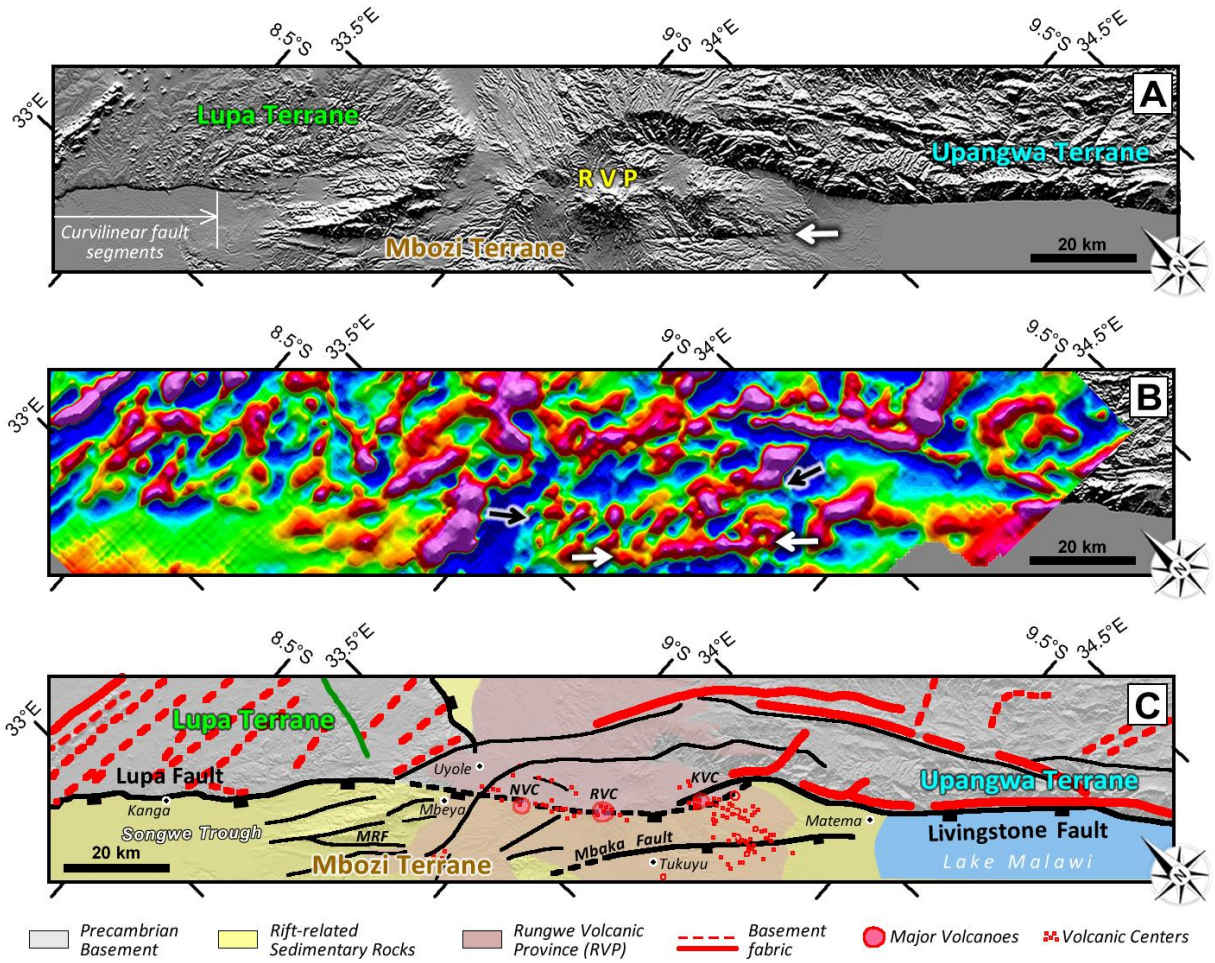

Fig. 11. The southern section of the Lupa Fault, the NE margin of the Mbozi Block (Rungwe Volcanic Province) and a section of the Livingstone Fault (NE border fault if the North Malawi Rift. Topographic digital elevation model in the top panel (A), the vertical derivative of the magnetic data in the middle panel (B), and a structural interpretation in the bottom panel (C). KVC = Kyejo Volcanic Center; NVC = Ngozi Volcanic Center; RVC = Rungwe Volcanic Center. Volcanic centers from Fontijn et al. (2010, 2012).

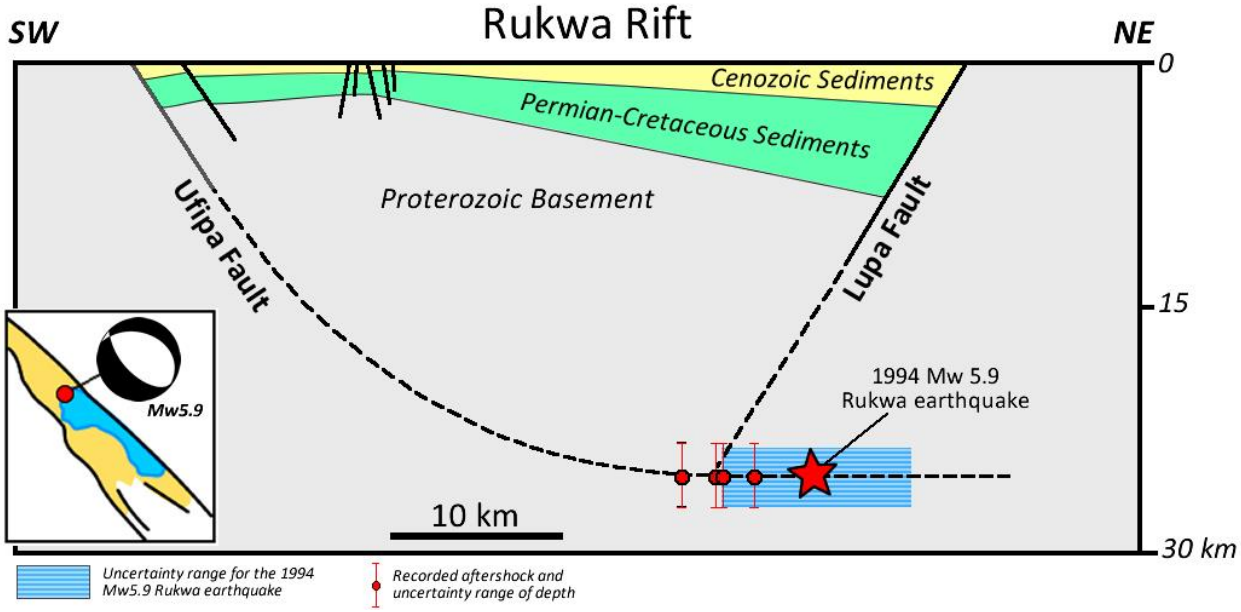

Fig. 12. Generalized geometrical relations of stratigraphic units and normal faults of the Rukwa rift, showing thickening of Cenozoic sediments towards both the Lupa and Ufipa border faults (modified after Zhao et al., 1997).

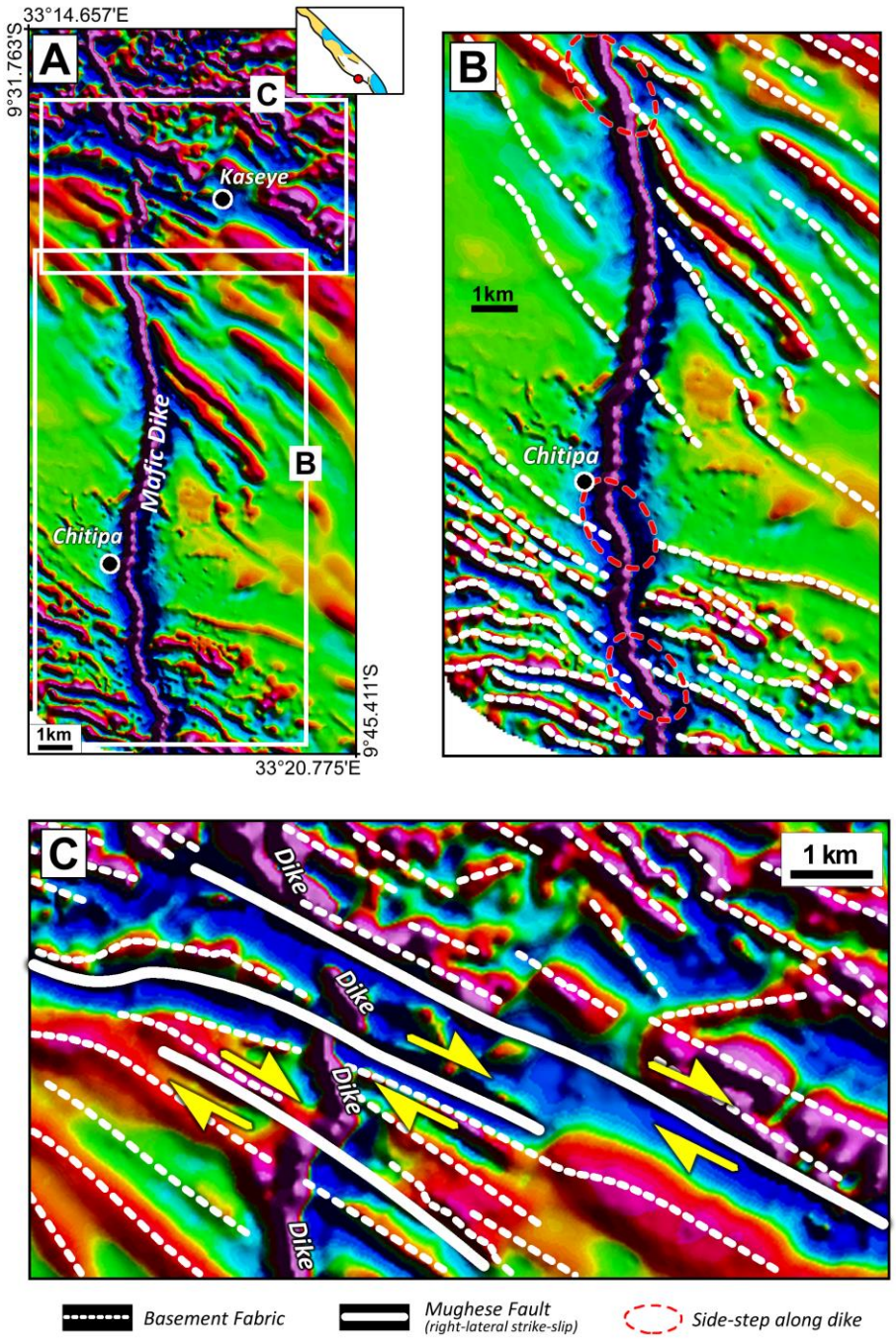

Fig. 13. (A) 1st vertical derivative of the aeromagnetic data covering the Kaseye-Chitipa area along the SW margin of the Mbozi Block (see location in top-right inset map, Figures 4A-B and 8C). (B) Close-up of the central and southern segments of a buried mafic dike (the "Chitipa Dike") showing side-stepping segments that coincide with pre-existing basement fabric. (C) Close-up of the northern segment of the dike showing right-lateral offsets by the continuation of the Ufipa Fault. This strike-slip fault segment is here-in referred to as the Mughese Fault.

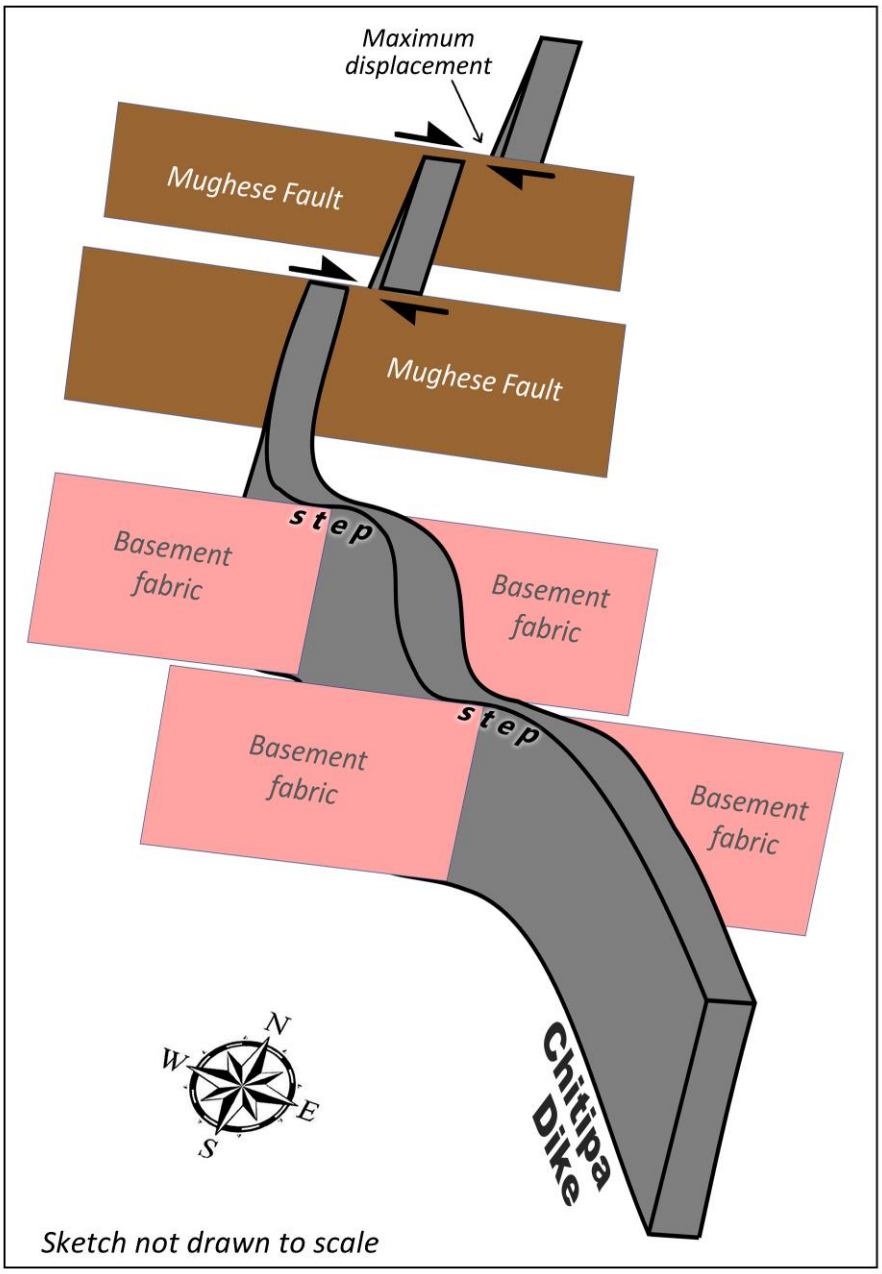

Fig. 14. 3-dimensional (3-D) conceptual model of the geometry of the interpreted dike (the "Chitipa Dike") and its interactions with the pre-existing basement fabric and the post-emplacement Mughese strike-slip fault offset.

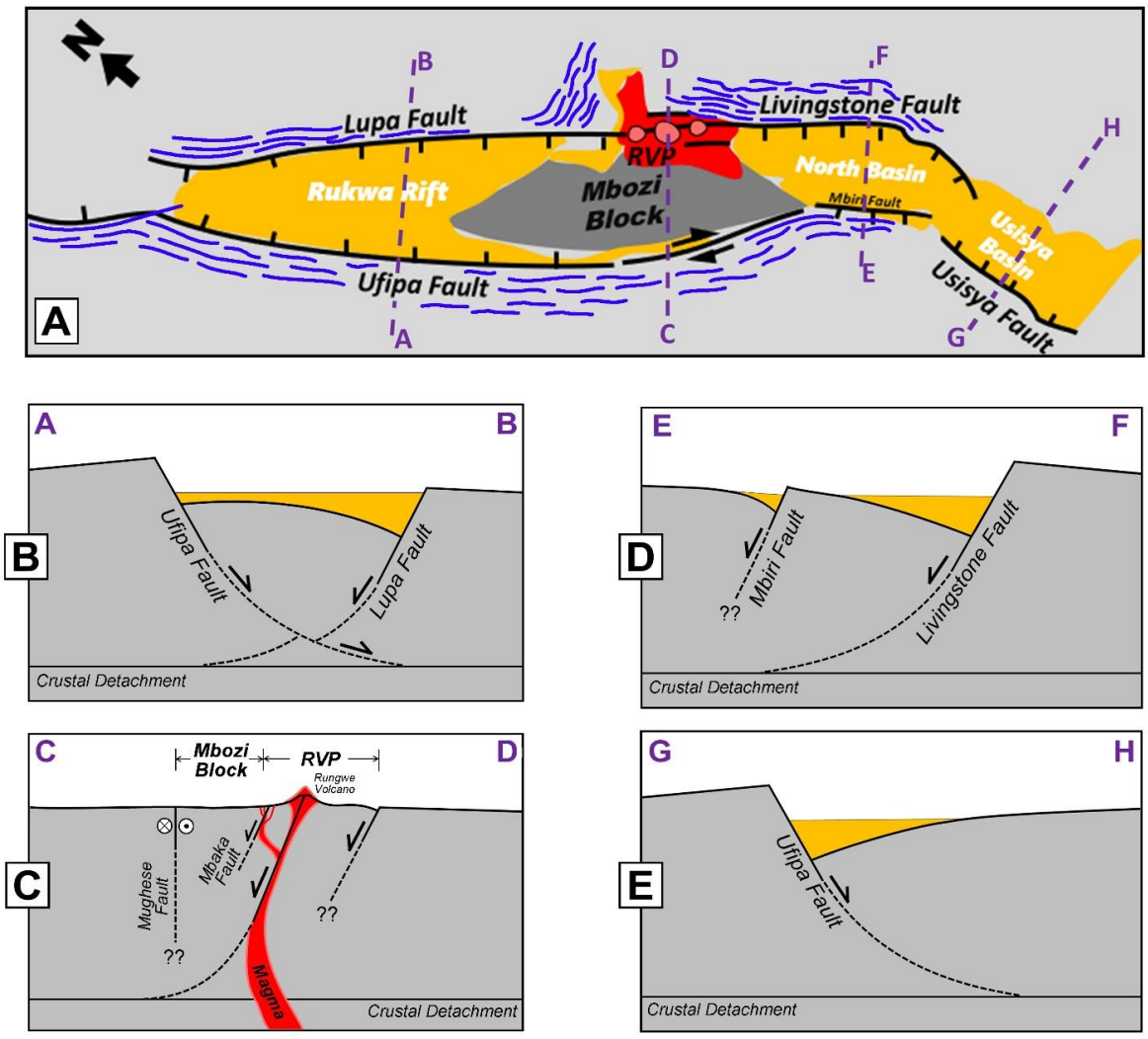

Fig. 15. (A) Generalized cartoon (map view) of the Rukwa-North Malawi Rift Segment (RNMRS) illustrating the continuous structural connectivity along the northeast and southwest boundaries, guided by the basement fabric. Black solid line = fault, blue solid line = basement fabric. RVP = Rungwe Volcanic Province. (B-E) Cross-section cartoons across the segments of the RNMRS, illustrating the possible subsurface geometries and interactions of the domain-bounding structures. LLF = Livingstone-Lupa Fault.

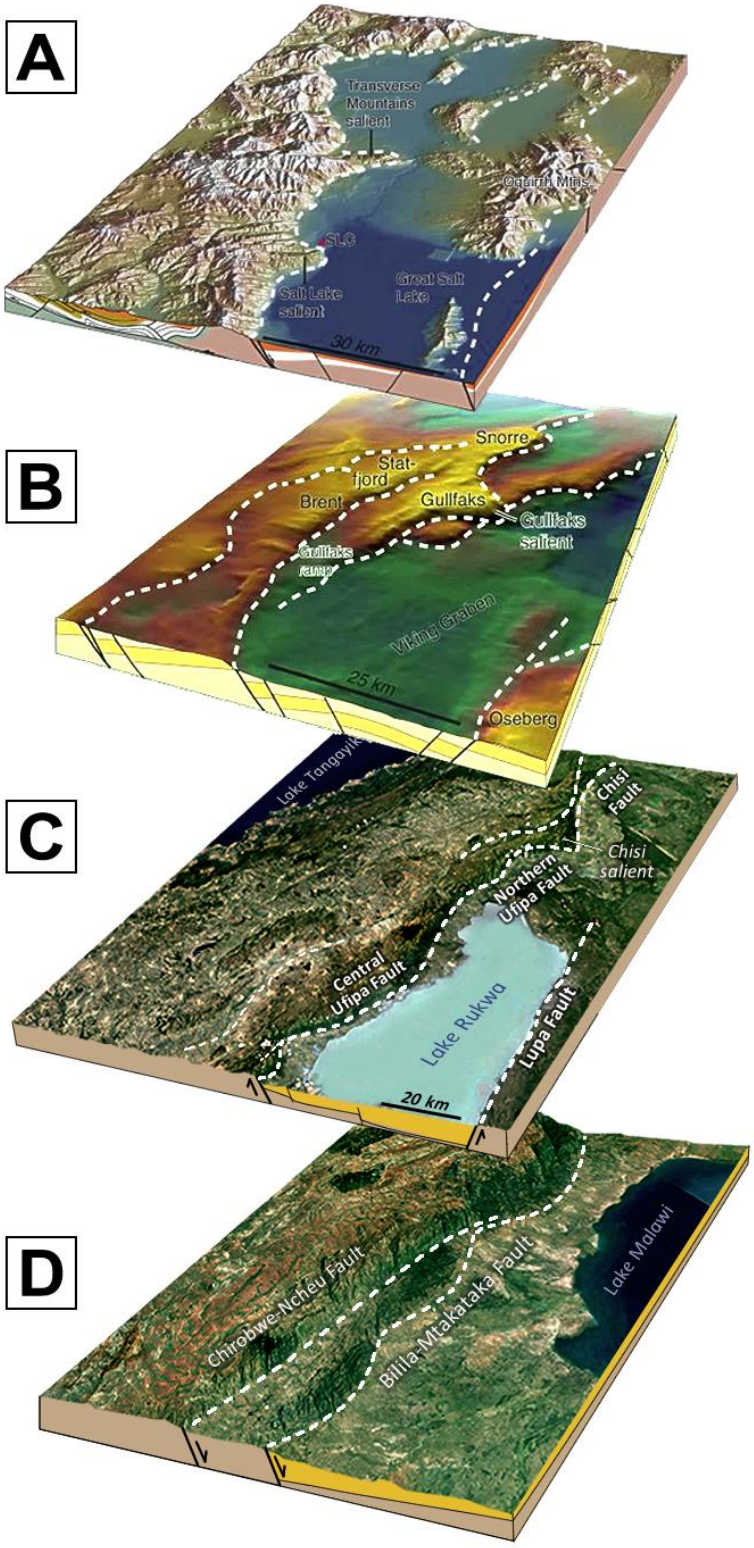

Fig. 16. (A-B) The Wasatch Fault in the Salt Lake area, Utah, and the first-order faults in the northern North Sea (base Cretaceous unconformity) showing concave-curvilinear fault geometries (modified after Fossen and Rotevatn, 2016). (C) Strikingly similar Concave-curvilinear fault geometry occurs in the northern Ufipa Fault and Chisi Fault in the Rukwa Rift. However, the Central Ufipa Fault shows convex-curvilinear fault geometry. (D) The Bilila-Mtakataka Fault also shows excellent convex curvilinear fault geometries.

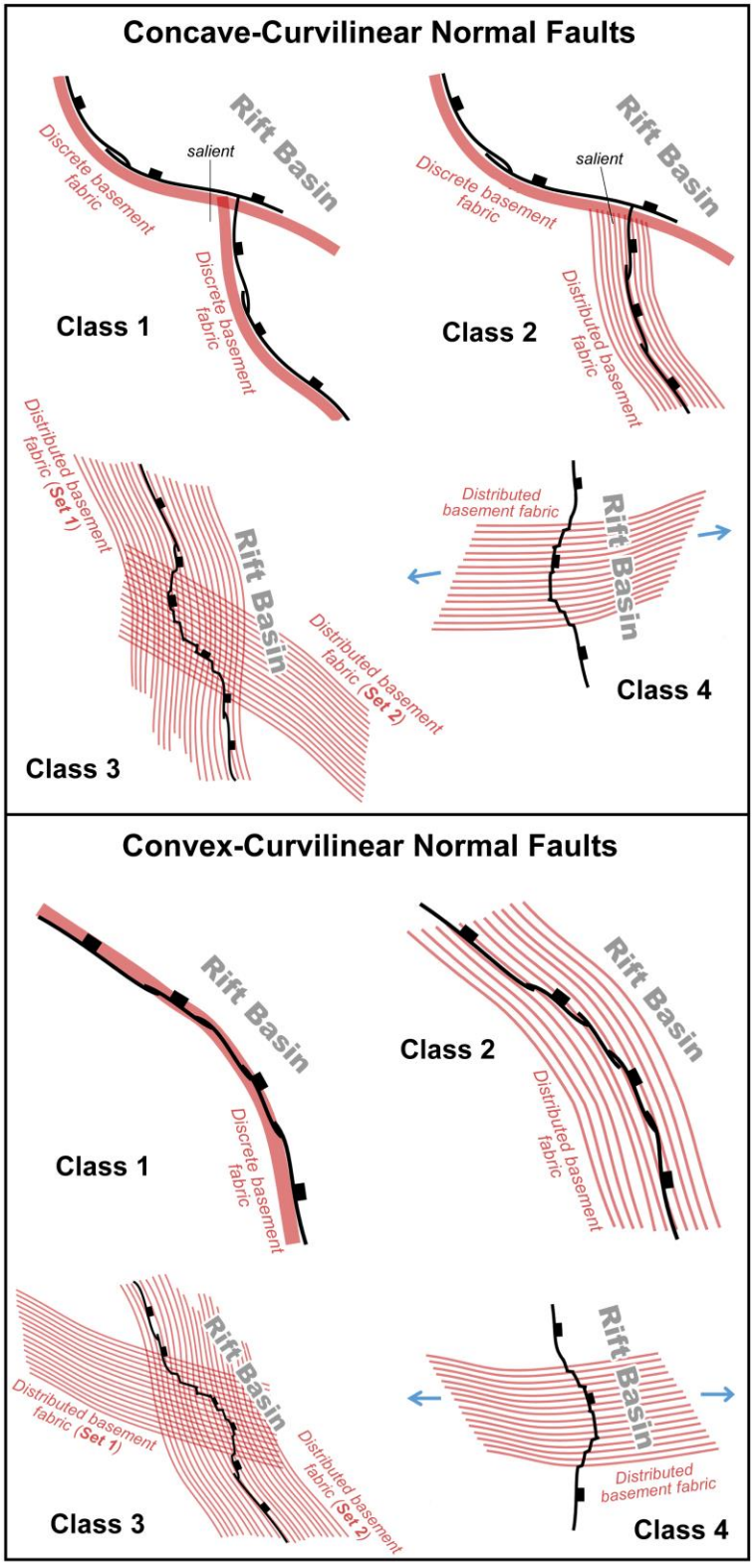

Fig. 17. Models illustrating the control of varying configurations of pre-existing basement fabrics on the development of concave- and convex-curvilinear normal fault plan-view geometries. These models are based on the observations from the Rukwa – North Malawi Rift Segment (this study).

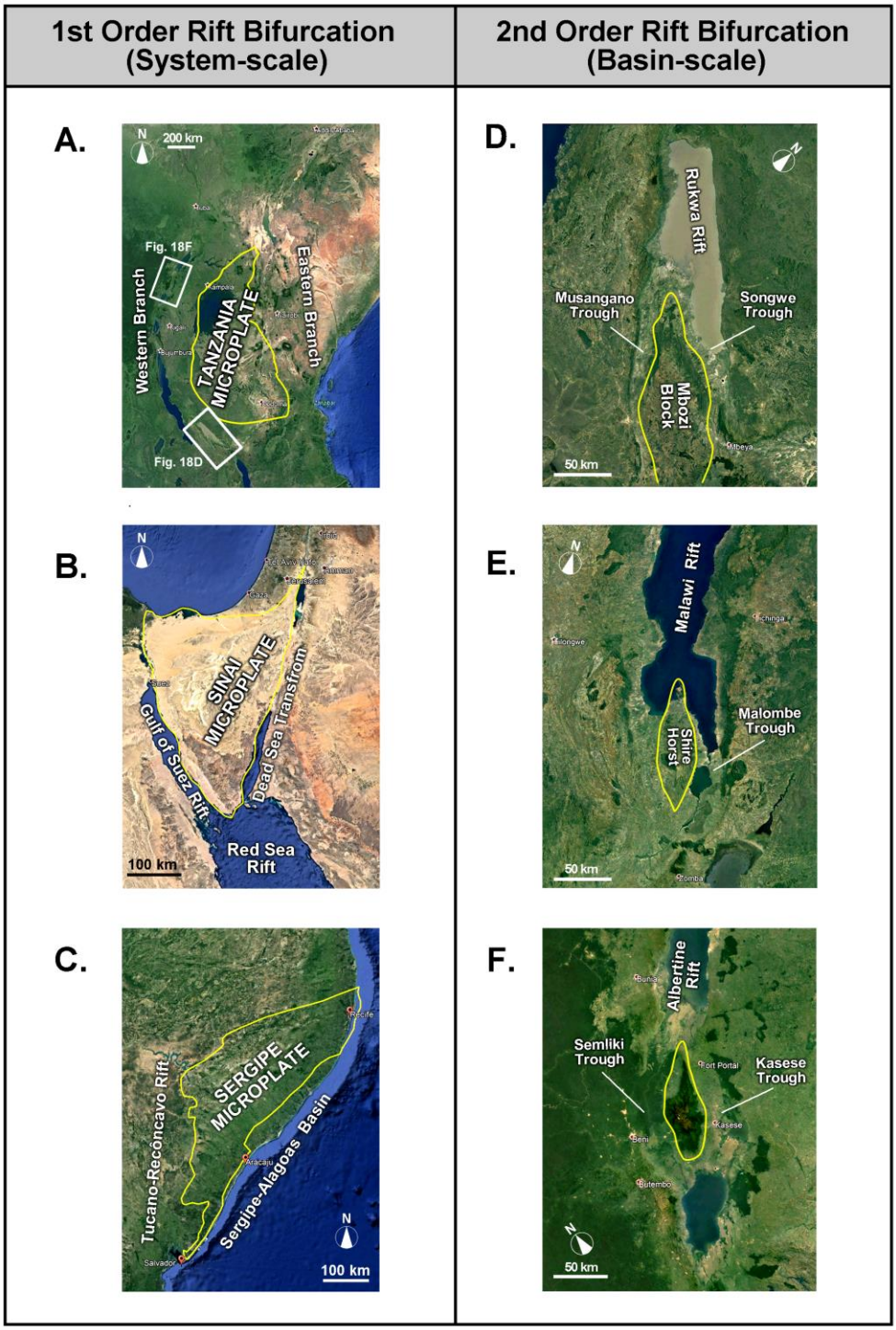

Fig. 18. Examples of system-scale rift bifurcation in the (A) East African Rift System, (B) Red Sea Rift and (C) South Atlantic Rift; and examples of basin-scale rift bifurcation in the (D) Rukwa Rift (see Fig. 18A for location), (E) southern Malawi Rift and (F) Albertine Rift (see Fig. 18A for location). These examples show that the 2nd order bifurcations are integral components of inter-rift transfer zones where the coupling of rift segments take place.